

RICE UNIVERSITY

**Gas Chromatography Study of Sulfur Removal from Jet Fuel
Using Nanoporous Materials**

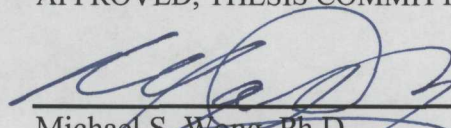
by

Samantha Kathiuska Samaniego Andrade

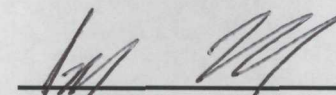
A THESIS SUBMITTED
IN PARTIAL FULFILLMENT OF THE
REQUIREMENTS FOR THE DEGREE

Master of Science in Chemical Engineering

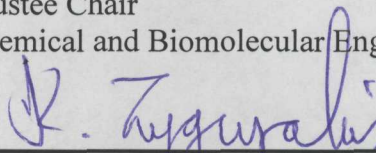
APPROVED, THESIS COMMITTEE



Michael S. Wong, Ph.D.,
Professor and Department Chair
Chemical and Biomolecular Engineering,
Chemistry, Materials Science and
Nanoengineering



Amanda Marciel, Ph.D.,
Assistant Professor, William Marsh Rice
Trustee Chair
Chemical and Biomolecular Engineering



Kyriacos Zygourakis, Ph.D.,
A.J. Hartsook Professor,
Chemical and Biomolecular Engineering

HOUSTON, TEXAS

June 2019

Copyright

Samantha Kathiuska Samaniego Andrade

2019

ABSTRACT

Gas Chromatography Study of Sulfur Removal from Jet Fuel Using Nanoporous Materials

by

Samantha Kathiuska Samaniego Andrade

Adsorptive desulfurization has been studied as a promising process to produce low-sulfur liquid fuels that achieve more stringent regulations. Although the process has proved to be effective to remove sulfur compounds from liquid fuels, a deep understanding of how the desulfurization occurs is still missing. In this work, gas chromatography coupled with Pulsed Flame Photometric Detector, GC-PFPD, is used to analyze the sulfur content of Jet Fuel samples before and after adsorptive desulfurization using nanoporous adsorbents at different temperatures (30°C - 180°C). The work aims to investigate if the adsorptive removal is selective to a certain fraction of sulfur compounds in the matrix of Jet Fuel. Also, the effect of temperature on the sulfur removal is studied. It was observed that on jet fuel, sulfur removal increases with temperature, reaching the highest sulfur removal at 180°C when using CuNa-Y zeolite (Dias da Silva, Samaniego Andrade, Zygourakis, & Wong, 2019). Sequential desulfurization experiments were done to see if the adsorbent can remove all sulfur compounds from jet fuel. At first, selectivity for the lighter sulfur compounds was observed, but after 4 desulfurization steps, all sulfur compounds were removed. This showed the adsorbent can remove all types of sulfur compounds in the matrix of jet fuel no matter their size.

Additionally, other materials were tested to evaluate their performance at desulfurization of jet fuel. The materials of choice were three metal organic frameworks (MOFs); the first one is UiO-66, and the other two materials were a modified version of UiO-66, named UiO-66-10 and UiO-66-25, which were prepared with a higher content of hydrochloric acid (HCl), 10% and 25% respectively, to create defects in the structure of the pristine UiO-66. UiO-66 was selected for this work because of its high porosity and for having a pore size bigger than that of CuNa-Y zeolite. In the series of UiO-66 materials, UIO-66-10 showed the best sulfur removal which also increased with increasing temperature, reaching its maximum capacity at 180°C. However, CuNa-Y zeolite still achieves a higher sulfur capacity than UIO-66-10. All the treated samples were analyzed through GC-PFPD to check on any change in the sulfur matrix of jet fuel. In the case of UIO-66 materials, selectivity towards lighter sulfur compounds was observed and this increases as the temperature of treatment increases. This behavior was also observed for the samples treated with CuNa-Y zeolite.

Acknowledgments

First, I thank God for keeping me healthy and motivated, for all the challenges that shape my life and make me grow stronger, and for all the many gifts I receive from him daily.

I would like to thank my research director Dr. Michael S. Wong, Chair of the Department of Chemical and Biomolecular Engineering at Rice University. I could not have come all this way if he had not trusted in my potential. When I first contacted him three years ago, Dr. Wong emailed me back to know better about my research interests and he encouraged me to apply to the Master of Science program in Chemical Engineering at Rice. I will always be grateful for his support. Looking back to my first days at Rice, I realize how much I have grown professionally but also personally. Dr. Wong helped me to improve and develop new skills while working with him. It was truly challenging to meet his expectations, but I learned how to overcome my own fears and worked hard to accomplish my goal.

Once in Dr. Wong's research group, I met a group of highly talented young researchers who are going through the challenges of their Ph.D. enthusiastically. They have inspired me to not limit myself on what I can achieve. I would like to especially thank Priscilla Dias da Silva for her collaboration, help, and advice while developing my own work. Also, I would like to thank Chelsea Clark for sharing with me part of her knowledge of H₂-Temperature Programmed Reduction and the synthesis of the UiO-66 metal-organic framework. To Yan Xu and Kimberly Heck, my officemates, for all the conversations that cheered up my mood when days went

rough. And to the rest of the group, who in one way or another gave me a hand during my journey.

I want to express my profound gratitude to Jacob Arredondo, Undergraduate Laboratory Supervisor of the Department of Chemical and Biomolecular Engineering at Rice University. I do not exaggerate when saying that Jacob was a lifesaver to me. He dedicated a lot of his time and effort to fix the gas chromatographer I used for my research, and he was always willing to answer my multiple questions and doubts. My knowledge of gas chromatography and the pulsed flame photometric detector has increased significantly thanks to our many discussions. I will always be in debt with Jacob, for his commitment, empathy, and guidance.

It is well known that distance is hard when one is far away from their loved ones. But, in these past two years, I have realized how distance is also a tool that teaches us to value what really matters in life, which for me is home and family. I am so thankful for how my family has supported my decision to come abroad and work for my dreams even though that meant for us to live separate. My parents, Isabel and Carlos, are the true responsible for my achievements. They were happy to see their little girl reading eagerly and asking many questions, and they never stopped me or tried to change my mind about my goals and expectations. Instead, they have worked so hard and dedicated their lives to give my siblings and me the best education possible. Thank you is not enough to express the gratitude I owe them. My siblings Andrea, Bryan, and Juliam are the best team ever. We all live separate now,

but we keep ourselves close in heart. I would like to especially thank Juliam, who is the funniest, most charismatic, creative, strong, and smart little person I know. His stories and laughs remind me that each day is worth it, and that distance is not a problem when love is pure.

To my dear friends Samuel, María Claudia, and Rosa. Thank you! for sharing your incredibly amazing personalities with me. I cannot count the many laughs we have shared, which made this whole adventure way easier and funnier. You are part of my family now and I am truly thankful for all our memories.

I would like to acknowledge the Fulbright Commission in Ecuador and their Fulbright Faculty Development Program for the financial support given along my master's program. Being a Fulbright scholar is an honor which I am thankful for, and all the learning that has resulted from this experience is an invaluable gift I will treasure all my life.

Last, I would like to dedicate this work in loving memory of Dr. Yosslen Rafael Aray Paraguan, who was my first research advisor and the person who encouraged me to trust myself and to keep working to leave my print in science.

Contents

Acknowledgments	iv
Contents.....	vii
List of Figures	x
List of Tables.....	xiv
List of Equations	xv
Nomenclature	xvi
Adsorptive Desulfurization of Jet Fuel	1
1.1. Jet Fuel.....	2
1.1.1. Composition of Jet Propellant 8 (JP-8).....	2
1.1.2. Current desulfurization methods.....	5
1.2. Adsorptive desulfurization applied to desulfurizing JP-8.....	7
1.2.1. Desired properties of adsorbents	7
1.2.2. Current limitations of adsorptive desulfurization of JP8.....	9
1.3. Nanoporous adsorbent materials: Sodium Y zeolite (Na-Y)	10
1.3.1. Structure of Na-Y, and surface properties	10
1.4. Nanoporous adsorbent materials: Metal-organic frameworks.....	13
1.4.1. Structure of UiO-66.....	14
1.4.2. Introduction of defects in UiO-66 structure	16
1.5. Gas chromatography.....	17
1.5.1. Application of gas chromatography to the study of adsorptive desulfurization of liquid fuels.....	17
1.5.2. Pulsed Flame Photometric Detector (PFPD)	18
1.6. Research objectives.....	23
Gas chromatography study of the adsorptive desulfurization of JP-8 using CuNa-Y zeolite.....	25
2.1. Description	25
2.2. Experimental work.....	26
2.2.1. Preparation of zeolitic materials.....	26
2.2.2. Characterization of Na-Y and CuNa-Y zeolites: XRD patterns	28

2.2.3. Preparation of fuel samples: JP-8.....	28
2.2.4. Batch desulfurization of jet fuel at elevated temperatures.....	28
2.2.5. Total sulfur content measurement.....	29
2.2.6. GC-PFPD test of treated JP-8 samples	30
2.2.7. Desulfurization of jet fuel by several desulfurization steps at 180°C.....	32
2.3. Description of results and analysis	33
2.3.1. Characterization of Na-Y and CuNa-Y zeolites: XRD patterns	33
2.3.2. Batch desulfurization of jet fuel at elevated temperatures.....	35
2.3.3. GC-PFPD test of treated JP-8 samples	37
2.3.4. Desulfurization of jet fuel by several desulfurization steps at 180°C.....	43
2.4. Conclusions.....	46
Study of the role of Copper species in adsorptive desulfurization using CuNa-Y zeolite	47
3.1. Introduction	47
3.2. Experimental work.....	48
3.2.1. Preparation of Cu(I)Na-Y and Cu(II)Na-Y zeolites	48
3.2.2. Characterization of Cu(I)Na-Y and Cu(II)Na-Y zeolites: XRD patterns and Hydrogen Temperature Programmed Reduction (H₂ -TPR) experiments	49
3.2.3. Preparation of fuel samples: Model fuels and JP-8.....	51
3.2.4. Batch desulfurization of fuels at elevated temperatures.....	52
3.2.5. Total sulfur content measurement.....	53
3.2.6. GC-PFPD test of treated JP-8 samples	53
3.3. Description of results and analysis	53
3.3.1. Characterization of Cu(I)Na-Y and Cu(II)Na-Y zeolites: XRD patterns and H₂ -TPR results	53
3.3.2. Batch desulfurization of model fuels at elevated temperatures	60
3.3.3. Batch desulfurization of JP8 at elevated temperatures.....	62
3.3.4. GC-PFPD test of treated JP-8 samples	64
3.4. Conclusions.....	67
Adsorptive desulfurization of JP-8 using UiO-66 metal-organic frameworks (MOFs).....	68
4.1. Introduction	68
4.2. Experimental work.....	69

4.2.1. Synthesis of UiO-66 metal-organic framework adsorbents	69
4.2.1.1. Synthesis of UiO-66-10 and UiO-66-25 adsorbents.....	70
4.2.1.2. Synthesis of UiO-66-DF adsorbent	71
4.2.2. Characterization of UiO-66 metal-organic framework adsorbents.....	73
4.2.3. Batch desulfurization of JP-8 at elevated temperatures	74
4.2.4. Total sulfur content measurement.....	74
4.2.5. GC-PFPD test of treated JP-8 samples	74
4.3. Description of results and analysis	75
4.3.1. Characterization of UiO-66 adsorbents: XRD patterns and surface properties.....	75
4.3.2. Batch desulfurization of JP-8 at elevated temperatures	78
4.3.3. GC-PFPD test of treated JP-8 samples	80
4.4. Conclusions.....	83
Future work	85
References	89

List of Figures

Figure 1.1.2-1. Hydrodesulfurization process of thiophene over unsupported solid Molybdenum Sulfide catalyst. In the case of trimethylbenzothiophene, which is a sterically hindered organosulfur compound, the process is less effective because the sulfur atom cannot reach the catalyst's active site (Tran et al., 2018).	5
Figure 1.2.2-1. Summary of the adsorption capacity of different materials towards organo-sulfur compounds present in JP-8. Most of the values reported correspond to light fractions of JP-8 with lower sulfur concentrations (Tran, 2018).	10
Figure 1.3.1-1. Detailed diagram of the structure of zeolite Y or faujasite. The locations of the oxygen framework atoms are labeled with the number 1 – 4. The roman numbers indicate the different designations and positions for the cations. The vertices in the structure of the zeolite correspond to T-atoms (T = Si/Al); the projection is along [111] (Klein, Kirschhock, & Fuess, 1994).	12
Figure 1.4.1-1. Structure of UiO-66 metal-organic framework. (a) Model of a super tetrahedron cage, (b) model of a super octahedron cage, (c) UiO-66 cubic unit consisting of eight inorganic Zr₆O₄(OH)₄ bricks; the cubic unit results from the combination of one octahedral cage and two adjacent tetrahedral cages. Atoms in structure are represented as follows: zirconium (red), oxygen (blue), carbon (gray), and hydrogen (white) (Valenzano et al., 2011).	15
Figure 1.4.1-2. From left to right: Comparison of the dimension of linker molecule, [001] view of UiO-66 metal-organic framework, tetrahedral cage, and octahedral cage (Chavan et al., 2012).	16
Figure 1.5.2-1. Combustor design and wall gas pathways (O.I. Analytical, 2004).	19
Figure 1.5.2-2. PFPD flame cycle (O.I. Analytical, 2004).	20
Figure 1.5.2-3. Lifetimes of carbon, phosphorus, and sulfur emissions (O.I. Analytical, 2004).	22
Figure 2.3.1-1. Experimental and simulated XRD patterns for Na-Y and CuNa-Y zeolites.	34
Figure 2.3.2-1. Total sulfur removed from JP-8 at 30°C, 80°C, 130°C, and 180°C by CuNa-Y and Na-Y zeolites. Initial sulfur concentration of JP-8 was 2230 ppmw _S . Retrieved data from: (Dias da Silva et al., 2019).	36

- Figure 2.3.3-1. Gas chromatograms (pulsed flame photometric detection) of thiophene, benzothiophene, 3-methylbenzothiophene, and dibenzothiophene (top) and chromatogram of sulfur compounds present in fresh JP-8 (bottom). The concentration of the thiophene, benzothiophene, 3-methylbenzothiophene, and dibenzothiophene samples was 25 ppmw_S each. The samples were prepared diluting the pure model sulfur compound in iso-octane. The JP-8 samples was used as received, its concentration was 2230 ppmw_S. Retrieved data from: (Dias da Silva et al., 2019)..... 38
- Figure 2.3.3-2. GC-PFPD results for JP-8 treated with CuNa-Y zeolite. From top to bottom: Untreated JP-8, JP-8 treated at 30°C, 80°C, 130°C, and 180°C. Retrieved data from: (Dias da Silva et al., 2019) 39
- Figure 2.3.3-3. GC-PFPD results for JP-8 treated with Na-Y zeolite. From top to bottom: Untreated JP-8, JP-8 treated at 30°C, 80°C, 130°C, and 180°C. Retrieved data from: (Dias da Silva et al., 2019). 41
- Figure 2.3.3-4. GC-PFPD results for JP-8 treated only by heating. From top to bottom: Untreated JP-8, JP-8 heated at 30°C, 80°C, 130°C, and 180°C. Retrieved data from: (Dias da Silva et al., 2019). 42
- Figure 2.3.4-1. Chromatograms of JP-8 samples after four consecutive desulfurization steps. From top to bottom: Untreated JP-8, first to fourth desulfurization steps. CuNa-Y zeolite pellets were used as adsorbent material. The total sulfur content for each fuel sample was measured by XRF. Chromatograms were obtained by GC-PFPD. Retrieved data from: (Dias da Silva et al., 2019) 43
- Figure 2.3.4-2. Step D in the series of four desulfurization steps of JP-8. CuNa-Y zeolite pellets were used as adsorbent material. The chromatogram was obtained by GC-PFPD using an attenuation factor of 1. Retrieved data from: (Dias da Silva et al., 2019) 45
- Figure 3.3.1-1. Measured XRD patterns of zeolitic materials. From top to bottom: Cu(II)Na-Y, Cu(I)Na-Y, CuNa-Y, Na-Y zeolites compared to the simulated XRD pattern of Na-Y zeolite. All XRD measurementst were done under ambient conditions. 54
- Figure 3.3.1-2. **H₂**-TPR curves for Cu(I)Na-Y zeolite. a) **H₂**-TPR analysis after in-situ activation of Cu(I)Na-Y zeolite. b) **H₂**-TPR analysis after ex-situ activation of Cu(I)Na-Y zeolite..... 55

Figure 3.3.1-3. H₂ -TPR curves for Cu(II)Na-Y zeolite. a) H₂ -TPR analysis after in-situ activation of Cu(II)Na-Y zeolite. b) H₂ -TPR analysis after ex-situ activation of Cu(II)Na-Y zeolite.	56
Figure 3.3.2-1. Total sulfur removed from MF versus temperature. Adsorbent materials were: squares-solid line for Cu(I)Na-Y, and dots-dashed line for Cu(II)Na-Y zeolite. The fuel used was MF (n-dodecane + 3MBT), 2000 ppmwS. Desulfurization time was 6 hours at 30°C, 80°C, 130°C, and 180°C.....	61
Figure 3.3.2-2. Total sulfur removed from MFT versus temperature. Adsorbent materials were: squares-solid line for Cu(I)Na-Y, and dots-dashed line for Cu(II)Na-Y zeolite. The fuel used was MFT (n-dodecane + 3MBT + 15%w toluene), 2000 ppmwS. Desulfurization time was 6 hours at 30°C, 80°C, 130°C, and 180°C.....	62
Figure 3.3.3-1. Total sulfur removed from JP-8 versus temperature. Adsorbent materials were: squares-solid line for Cu(I)Na-Y, and dots-dashed line for Cu(II)Na-Y zeolite. The fuel used was JP-8, 2230 ppmwS. Desulfurization time was 6 hours at 30°C, 80°C, 130°C, and 180°C.	63
Figure 3.3.4-1. GC-PFPD results for JP-8 treated with Cu(I)Na-Y zeolite. From top to bottom: Untreated JP-8, JP-8 treated at 30°C, 80°C, 130°C, and 180°C.....	65
Figure 3.3.4-2. GC-PFPD results for JP-8 treated with Cu(II)Na-Y zeolite. From top to bottom: Untreated JP-8, JP-8 treated at 30°C, 80°C, 130°C, and 180°C.....	66
Figure 4.2.1-1. Procedure for the synthesis of defective UiO-66 adsorbents (UiO-66-10 and UiO-66-25).....	71
Figure 4.2.1-2. Procedure for the synthesis of defect-free UiO-66 adsorbent (UiO-66-DF)	73
Figure 4.3.1-1. Measured XRD patterns of UiO-66 metal-organic framework adsorbents. The simulated XRD pattern of pristine UiO-66 is also shown for comparison.....	76
Figure 4.3.1-2. [001] view of fcu UiO-66 metal-organic framework. Atoms are colored as follows: O, red; Zr, blue; C, grey; H, white. Model was produced using the software Mercury 3.10.3 provided by The Cambridge Crystallographic Data Centre (CCDC).....	76
Figure 4.3.2-1. Total sulfur removed from JP-8 versus temperature. Adsorbent materials were: diamond-dots line for CuNa-Y zeolite, triangles-dash line for UiO-	

66-10, squares-solid line for UiO-66-25, circles-dash line for UiO-66-DF, and solid dots-solid line for Na-Y zeolite. The fuel used was JP-8, 2230 ppmwS. Desulfurization time was 6 hours at 30°C, 80°C, 130°C, and 180°C..... 79

Figure 4.3.2-2. GC-PFPD signal for JP-8 treated with UiO-66-10 metal-organic framework. From top to bottom: Untreated JP-8, JP-8 treated at 30°C, 80°C, 130°C, and 180°C..... 81

Figure 4.3.2-3. GC-PFPD signal for JP-8 treated with UiO-66-25 metal-organic framework. From top to bottom: Untreated JP-8, JP-8 treated at 30°C, 80°C, 130°C, and 180°C..... 82

Figure 4.3.2-4. GC-PFPD signal for JP-8 treated with UiO-66-DF metal-organic framework. From top to bottom: Untreated JP-8, JP-8 treated at 30°C, 80°C, 130°C, and 180°C..... 83

Figure 4.3.2-1. Schematic illustration for the process of optimization and metalated ligand exchange in UiO-66..... 88

List of Tables

Table 1.1.1-1. Components of JP-8 (Bakshi & Henderson, 1998)	3
Table 1.1.1-2. Additives used in JP-8 (“Toxicol. Assess. Jet-Propulsion Fuel 8,” 2015)	3
Table 2.2.6-1. GC-PFPD system description	30
Table 2.3.1-1. Properties of zeolitic adsorbents (Patent No. WO2017100617A1, 2016)	35
Table 3.2.3-1. List of tested fuels	52
Table 3.3.1-1. Hydrogen consumption during <i>H2</i> -TPR analysis of Cu(I)Na-Y and Cu(II)Na-Y zeolites	58
Table 3.3.1-2. Quantification of copper species in Cu(I)Na-Y and Cu(II)Na-Y zeolites after in-situ and ex-situ activation. The results correspond to the percentage of each copper specie over the total copper mass in the respective zeolite sample.....	59
Table 4.3.1-1. Surface properties of synthesized UiO-66 adsorbents (Clark et al., 2019)	77

List of Equations

Equation 2.2.5-1. Amount of sulfur removed (Dias da Silva et al., 2019).....	29
Equation 3.2.2-1. Chemical mechanism for the reduction of copper species in CuNa-Y zeolite under hydrogen as reducing agent (Richter et al., 2007).....	50

Nomenclature

GC-PFPD	Gas chromatography coupled to Pulsed flame photometric detector
XRF	X-ray fluorescence
XRD	X-ray diffraction
Na-Y	Sodium Y zeolite
CuNa-Y zeolite	Cu ion-exchange sodium Y zeolite
H ₂ -TPR	Hydrogen Temperature Programmed Reduction
TCD	Thermal conductivity detector
Cu(I)	<i>Cu</i> ⁺ cation
Cu(II)	<i>Cu</i> ²⁺ cation
ms	millisecond
rpm	revolutions per minute
ppmw _S	parts per million of Sulfur (weight based)
UiO-66	Universitetet I Oslo
MOF	metal-organic framework

Adsorptive Desulfurization of Jet Fuel

Adsorptive desulfurization has been studied as a promising technique to reach ultra-low sulfur concentration in liquid fuels. Although the method has shown good results, most studies have been done using model fuels with sulfur concentrations lower than that of real fuels (Velu, Ma, & Song, 2003). Also, most work has been done at room temperature, therefore the effect of elevated temperature on adsorptive desulfurization is not clear yet. Several adsorbents have been tested depending on the type of sulfur compounds present in the tested fuels, the possible interactions that may favor sulfur removal (Hernández-Maldonado & Yang, 2004), (Herna & Yang, 2003), and the regenerability of the adsorbent after treatment.

Due to the availability of jet fuel, specifically JP-8, for all army operations, this fuel is the ideal choice to use in energy generation devices such as fuel cells to be used in military missions at remote locations. But a prevalent problem is the high

sulfur content in JP-8 that poisons the catalyst in the fuel cell's reformer (Tran, Palomino, & Oliver, 2018). To solve this issue, adsorptive desulfurization of JP-8 is being investigated to develop high sulfur capacity adsorbents, which are easily regenerable, and to determine the operation conditions to enhance this process.

1.1. Jet Fuel

Jet-fuel or also known as Aviation turbine fuel, is a type of fuel for use in turbofan, turbo jet, and turboprop engines. There are several types of jet fuel depending on its physical and chemical characteristics. The fuel used in this study is a Military Jet Fuel grade known as Jet-propulsion fuel 8 or JP-8 ("Shell Aviation Fuels," n.d.).

1.1.1. Composition of Jet Propellant 8 (JP-8)

JP-8 is a fuel widely used by the U.S. military. Although at first the fuel was used only for aircrafts, the military is moving to use it also for ground vehicles and most importantly for energy generation. Energy generation is of special interest for missions where the energy supply is scarce or non-existent and the use of portable energy generation devices is required.

JP-8 is a kerosene-based fuel; it is produced from other two aviation fuels, jet fuel A and jet fuel A-1, which are used in commercial flights. The composition of JP-8 also includes additives such as icing, static, and corrosion inhibitors. Antioxidants

and metal deactivators may also be added to the fuel if needed (“Toxicol. Assess. Jet-Propulsion Fuel 8,” 2015).

The average composition of JP-8 by volume is shown in Table 1.1.1-1, and the list of additives used in this fuel are shown in Table 1.1.1-2.

Table 1.1.1-1. Components of JP-8 (Bakshi & Henderson, 1998)

Specie	Volume %
$C_8 - C_9$ aliphatic hydrocarbons	≈ 9%
$C_{10} - C_{14}$ aliphatic hydrocarbons	≈ 65%
$C_{15} - C_{17}$ aliphatic hydrocarbons	≈ 7%
Aromatics (typical aromatics: benzene, alkyl benzenes, toluene, xylene, indenes, naphthalenes.	≈ 18%

Table 1.1.1-2. Additives used in JP-8 (“Toxicol. Assess. Jet-Propulsion Fuel 8,” 2015)

Additive	Function	Quantity	Required or Optional
Diethylene glycol monomethyl ether, (DiEGME)	Ice inhibition	0.1 vol%	Required

Stadis 450	Static inhibition	2 mg/L	Required
DCI-4A	Corrosion inhibition	15 mg/L	Required
Antioxidant	Gum formation inhibition	25 ppm	Optional
Metal deactivator	Control of metal-catalyzed fuel deterioration	3 ppm	Optional

The sulfur content in JP-8 depends on the refining facility, and it also varies from batch to batch. Since JP-8 is a fuel destined to military use, it does not have to comply so strict restrictions regarding its maximum sulfur concentration. The U.S Army follows the American Society of Testing and Materials standard MIL-DTL-83133E for JP-8, which demands a maximum sulfur content of 3000 ppm (Andrews, 2009). The type of organosulfur molecules found in JP-8 may vary depending on the producer, being alkylated benzothiophenes the most common sulfur compounds present in JP-8. For example, from the work by Ubanyionwu and coworkers, it is known that the two most representative sulfur compounds in samples of JP-8 obtained from Fort Belvoir, VA, were 2,3-dimethylbenzothiophene and 2,3,7-trimethylbenzothiophene (Lee & Ubanyionwu, 2008). The work by Baltrus and collaborators also identified 2,3-dimethylbenzothiophene and 2,3,7-

trimethylbenzothiophene as the major sulfur sources in jet fuel, with a lower amount of dibenzothiophene (Link et al., 2003).

1.1.2. Current desulfurization methods

Fossil fuels are mainly desulfurized by hydrodesulfurization or HDS. This method uses a feed of hydrogen gas at high temperature and pressure to activate a metal catalyst to create a coordinatively unsaturated site that can react with the sulfur atom in organosulfur compounds. The interaction of the sulfur atom with the catalyst releases hydrogen sulfide and the continue hydrogen feeding produces the hydrogenation of the sulfur-free molecule. For example, through HDS, a thiophene molecule transforms in butane with the production of hydrogen sulfide (Tran et al., 2018).

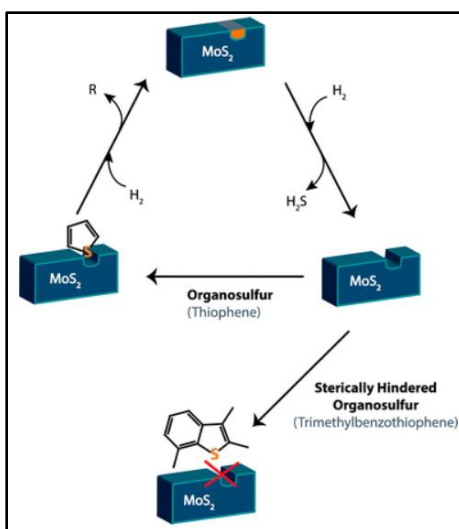


Figure 1.1.2-1. Hydrodesulfurization process of thiophene over unsupported solid Molybdenum Sulfide catalyst. In the case of trimethylbenzothiophene, which is a sterically hindered organosulfur compound, the process is less

effective because the sulfur atom cannot reach the catalyst's active site (Tran et al., 2018).

HDS works very well with lighter fuels such as gasoline. However, heavier fuels are more complicated to desulfurize through HDS because they contain organosulfur compounds such as alkylated benzothiophenes and dibenzothiophenes which are sterically hindered and cannot react with the catalyst. Therefore, these compounds remain in the fuel even after the HDS process, for what reason they are known as refractory sulfur compounds (Tran et al., 2018). A representation of the HDS process is shown in Figure 1.1.2-1.

As mentioned before, the HDS process requires high temperatures and pressures as well as big installations for the process to occur. However, as it was explained, the HDS process is not completely effective to remove the larger sulfur molecules such as benzothiophenes, alkylated benzothiophenes, or dibenzothiophenes. For those reasons, adsorptive desulfurization is being investigated as an effective process to remove those types of sulfur compounds. This process also results to be less complicated to operate as it does not need high pressures or extremely high temperatures to activate the removal of sulfur contaminants.

All the characteristics described above make adsorptive desulfurization an excellent alternative, specially to desulfurize fuels in remote locations where the access to specialized infrastructure is not possible. An example of this situation is the case of army operations in remote locations. In those cases, JP-8 may be used to

generate electricity. The fuel has a potential to be used as an energy source in energy generator devices such as solid oxide fuel cells (SOFCs) which can be used by the army forces in locations worldwide where the energy supply is limited or nonexistent (Tran et al., 2018).

A major drawback for the use of JP-8 in energy generations is its high sulfur content. Thus, adsorptive desulfurization offers the possibility to produce a low-sulfur fuel at relatively simple operation conditions. But for being used in fuel cells, liquid fuels must reach a sulfur content lower than 0.1 ppmw of sulfur (Bhandari et al., 2006).

1.2. Adsorptive desulfurization applied to desulfurizing JP-8

1.2.1. Desired properties of adsorbents

As described in the review prepared by Tran and coworkers (Tran, 2018), most materials used for desulfurization processes tend to be porous, cheap, and they are loaded with metals that enhance the desulfurization process.

The porosity of desulfurization materials is important since a porous structure provides a bigger surface area which results in more availability of space for the process to occur. Zeolites are the perfect example of these materials and they have been used widely as catalyst for the HDS process (Yi Wang, Wang, Rives, & Sun, 2014).

Besides porosity, adsorbent materials may be loaded with metal-active sites that are located over the framework of the adsorbent. A good example are the ion-exchanged zeolites that are loaded with transition metals such as nickel, silver, or copper and have shown good performance in desulfurization of liquid fuels (Hernández-Maldonado & Yang, 2004). As shown by Hernández-Maldonado and Yang, the addition of metal cations onto the structure of Na-Y-zeolite resulted in the production of low-sulfur fuels (< 4 ppmw_sulfur) which was not possible by using the pristine Na-Y zeolite.

The work by Velu and collaborators (Velu et al., 2003) presented the use of ion-exchanged NH_4Y zeolite for the desulfurization of a model and a real jet fuel. NH_4Y zeolite exchanged with cerium atoms showed the best results in the removal of benzothiophene molecules from jet fuel. Also, the concept of “Selective adsorption for removing sulfur (PSU-SARS)” was presented. According to this work, sulfur molecules may adsorb via direct sulfur-adsorbent interaction or via π -complexation. According to Velu and collaborators (Velu et al., 2003), the zeolite exchanged with cerium atoms performed via direct sulfur-adsorbent interaction rather than via π -complexation. These findings elucidated other aspects to be considered while choosing an adsorbent for adsorptive desulfurization. Adsorbents loaded with metal cations with the availability of electrons to form a π -complexation interaction may adsorb to aromatic compounds instead of organo-sulfur compounds like benzothiophenes; therefore, the right choice of metal cations to add to the zeolite framework is needed before starting the desulfurization process. This selection

depends on the type of sulfur compounds to be removed, and the competitor compounds such as aromatics present in the fuel.

1.2.2. Current limitations of adsorptive desulfurization of JP8

Although, adsorptive desulfurization of jet fuels has been studied increasingly in the past decade, most of those studies have been performed on model fuels rather than real fuels; or if real fuels were used, their sulfur content was considerably lower than that of the JP-8 used in this work (2230 ppmw_Sulfur) (Herna & Yang, 2003), (Hernández-Maldonado & Yang, 2004), (Yuhe Wang et al., 2006). Figure 1.2.2-1 presents a list of some of the different adsorbents studied for adsorptive desulfurization of JP-8 samples. It is worth noting that the values presented in Figure 1.2.2-1 correspond to the desulfurization of light fractions of JP-8 with much less sulfur to remove.

Sorbent	Initial ppm _w S of JP-8	Optimized adsorption capacity (mg S g ⁻¹)
Zn ²⁺ /zeolite Y	750	0
Cu ²⁺ /zeolite Y	750	0.3
MCM-41	517	0.8
H ⁺ /zeolite Y	750	1.3
Ni ²⁺ /zeolite Y	750	2.0
Pd ²⁺ /zeolite Y	750	2.6
Ce ³⁺ /zeolite Y	750	2.7
MSN	517	4.6
Au ⁺ /SiO ₂	6.6	5.7
Ag-TiO _x -Al ₂ O ₃	630	8.01
Ag-MCM-41	517	25.4
Ag-MSN	517	32.6
DDA-15	750	39.4
Ag-MASN	750	41.1

Figure 1.2.2-1. Summary of the adsorption capacity of different materials towards organo-sulfur compounds present in JP-8. Most of the values reported correspond to light fractions of JP-8 with lower sulfur concentrations (Tran, 2018).

1.3. Nanoporous adsorbent materials: Sodium Y zeolite (Na-Y)

1.3.1. Structure of Na-Y, and surface properties

Zeolites are crystalline aluminosilicates, formed by corner-sharing AlO_4 and SiO_4 tetrahedra connected in three-dimensional frameworks with pores of molecular dimensions. A framework formed entirely by silicon has neutral charge, but the presence of aluminum in the zeolite structure results in a negative charge which is balanced by the presence of cations. Because these cations are not fixed, they can be replaced by ion-exchange methods. Y zeolite belongs to the cubic space

group $Fd\bar{3}m$, with a lattice constant between 24.2 and 25 Å. The lattice constant value depends on the aluminum concentration of the framework, the type of cations, and the state of hydration of the zeolite (Kaduk, J.A.; Faber, 1995).

The structure of Y zeolite is formed by 24-tetrahedra cuboctahedral units, also known as SODALITE cages. The sodalite cages are joined together through hexagonal prisms or double 6-rings of oxygen (O) atoms. If compared to the diamond structure, the sodalite cages play the role of carbons atoms, while the double 6-rings play the role of the C-C bonds (Kaduk, J.A.; Faber, 1995).

The pore structure of Y zeolite is formed by super-cages of 12 Å in diameter. The super-cages are connected through small cavities of approximately 8 Å in diameter which are formed by 12 linked tetrahedra that form 12-rings formed by 12 Si/Al and 12 O atoms. This wide structure of cages and pores allows the diffusion of large molecules such as benzothiophenes. Therefore, Y zeolite is one of the most used materials for adsorptive desulfurization as well as catalytic applications. Y zeolite has a higher silicon content compared to its sister X zeolite which has a higher aluminum content (Kaduk, J.A.; Faber, 1995).

Figure 1.3.1-1 shows the positions of the extra-framework cations on the zeolite Y structure. The cations sites are designated by roman numerals from I to VI.

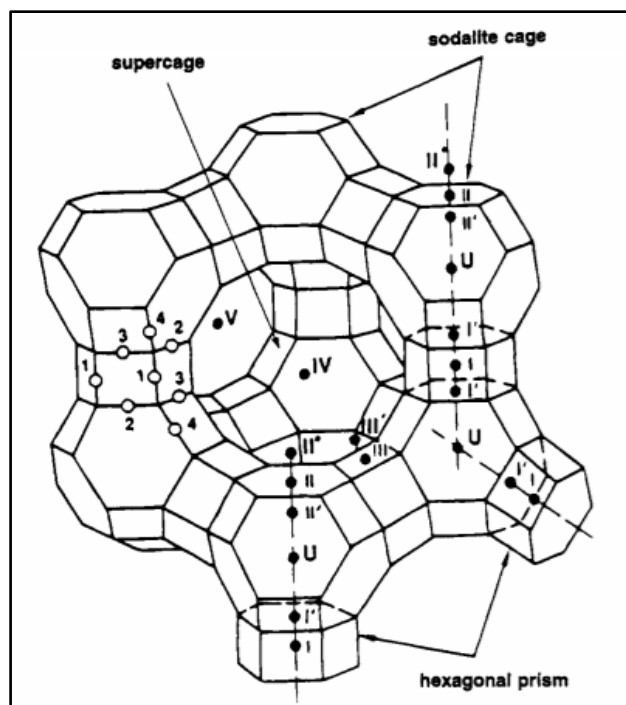


Figure 1.3.1-1. Detailed diagram of the structure of zeolite Y or faujasite. The locations of the oxygen framework atoms are labeled with the number 1 - 4. The roman numbers indicate the different designations and positions for the cations. The vertices in the structure of the zeolite correspond to T-atoms (T = Si/Al); the projection is along [111] (Klein, Kirschhock, & Fuess, 1994).

Since the present work uses copper ion-exchanged Na-Y zeolite, a brief description of the location of the copper cations is presented. According to the work by Drake and coworkers (Drake et al., 2006), in the framework of ion-exchanged CuNa-Y zeolite, the copper cations may occupy the positions I(I'), II(II'), which are located on the sodalite cavities, and site III(III') which is located on the super-cage.

The work by (Fowkes, Ibberson, & Rosseinsky, 2002) suggested that when copper cations are loaded to the zeolite Y structure via liquid ion-exchange, and then reduced from Cu(II) to Cu(I) under H_2 , the Cu(I) cations occupy the III(III')

sites. Since the III(III') sites are the ones exposed on the biggest pore in the structure of zeolite Y, the cations located on those sites are the more accessible to reactants and therefore are very active.

Ion-exchanged CuNa-Y zeolite has been reported as a good adsorbent for desulfurization purposes when applied to fuels such as gasoline and diesel, removing their sulfur content to less than 4 ppmw sulfur (Hernández-Maldonado & Yang, 2004). It has been claimed that at room temperature, the adsorptive desulfurization process with CuNa-Y zeolite is driven by the ability of the adsorbent to remove sulfur molecules through π -complexation (Herna & Yang, 2003). An important aspect to consider is that although the activation process of CuNa-Y zeolite aims to reduce the copper cations from Cu(II) to Cu(I), there is a portion of cations that stays as Cu(II). Cu(I) cations counts with the electrons needed to connect to aromatic sulfur compounds through π -complexation, while Cu(II) cations are more likely to bond through direct sulfur-metal bonds.

1.4. Nanoporous adsorbent materials: Metal-organic frameworks

Metal organic frameworks or MOFs are a whole new branch of porous materials which besides the benefit of large surface areas and porous structures, may be designed and tuned to accomplished specific tasks. Changing the synthesis methods of these materials may result in outstanding characteristics related to their chemical reactivity, stability, or novel structures that enhance their surface and

pores availability. MOFs are formed by inorganic bricks and organic complexing molecules which play the role of spacers that create voids or pores in three dimensional structures with high surface areas and pore volumes (Valenzano et al., 2011).

The different combinations of constituents in the synthesis of MOFs to achieve different geometries, variations in size, and functionalization of the structures, have led to the production of more than 20,000 different MOFs reported within the past decade (Furukawa, Cordova, O’Keeffe, & Yaghi, 2013).

The organic part in MOFs corresponds to ditopic or polytopic organic carboxylates, which are linked to metal-containing clusters. This combination results in architecturally robust crystalline MOF structures. A typical characteristic of these structures is a porosity that is greater than 50% of the MOF crystal volume. Regarding their surface areas, the values range from 1000 to 10,000 m^2/g which surpass the surface areas of other common porous materials such as zeolites, and carbons. Because of these properties, MOFs are materials of interest for applications such as capture of carbon dioxide, storage of fuels, and catalytic processes (Furukawa et al., 2013).

1.4.1. Structure of UiO-66

UiO-66 metal-organic framework is formed by $Zr_6O_4(OH)_4$ octahedron clusters, joined together by 1,4-benzene-dicarboxylate (BDC) linkers. Each

octahedron is 12-fold connected to its nearest octahedron (Valenzano et al., 2011).

Figure 1.4.1-1 displays the structure of the UiO-66 metal-organic framework.

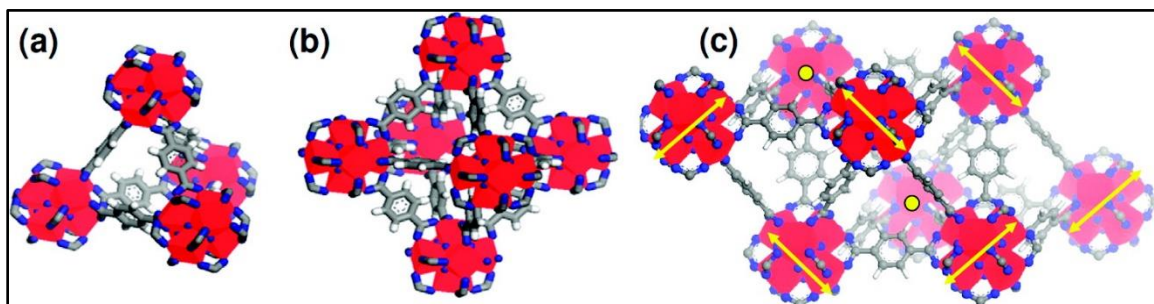


Figure 1.4.1-1. Structure of UiO-66 metal-organic framework. (a) Model of a super tetrahedron cage, (b) model of a super octahedron cage, (c) UiO-66 cubic unit consisting of eight inorganic $Zr_6O_4(OH)_4$ bricks; the cubic unit results from the combination of one octahedral cage and two adjacent tetrahedral cages. Atoms in structure are represented as follows: zirconium (red), oxygen (blue), carbon (gray), and hydrogen (white) (Valenzano et al., 2011).

Generally, MOFs have the disadvantage of having weak stability; their thermal stability ranges from 350 - 400°C. This condition makes them not suitable for all industrial applications. However, the UiO-66 metal-organic framework has attracted attention due to its unprecedented stability (derived from the strength of the Zr-O bond), chemical resistance and high surface area. UiO-66 can stand temperatures up to 540°C and its crystalline structure remains unaffected even after exposure to 10 tons/cm² of external pressure (Lillerud et al., 2008). Figure 1.4.1-2 shows the dimension of the 1,4-benzene-dicarboxylate linker compared to the diameter of the tetrahedral and octahedral cages of UiO-66 metal-organic

framework. The size of the 1,4-benzene-dicarboxylate linker gives the length of separation between the octahedron clusters.

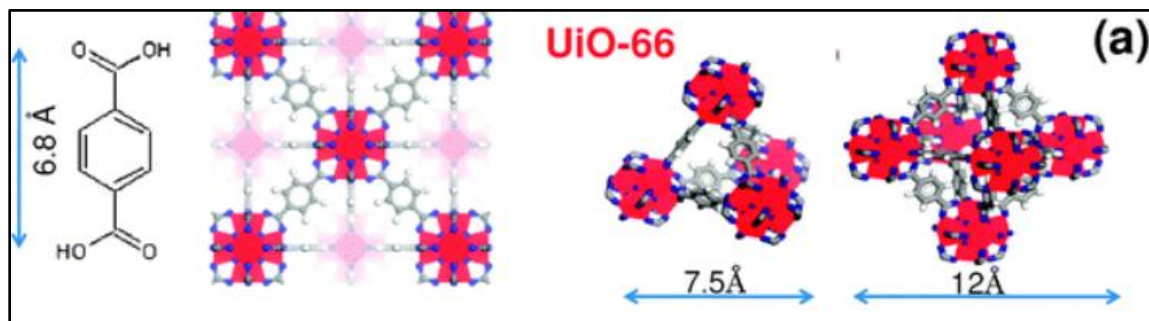


Figure 1.4.1-2. From left to right: Comparison of the dimension of linker molecule, [001] view of UiO-66 metal-organic framework, tetrahedral cage, and octahedral cage (Chavan et al., 2012).

1.4.2. Introduction of defects in UiO-66 structure

Structural defects can be introduced in the UiO-66 framework following the modulated synthesis approach, which has been used to produce adsorbent materials with increased porosity and a larger number of coordinatively unsaturated (CUS) Zr^{4+} sites. The availability of CUS- Zr^{4+} and an increased porosity can enhance the performance of the material for adsorption purposes. Two typical modulators are known: monodentate carboxylic acids and concentrated hydrochloric acid (conc. HCl). The first modulator, monodentate carboxylic acids, compete with the bidentate benzenedicarboxylate (bdc) ligands that connect the Zr nodes. The second modulator, HCl, has been reported as an accelerator to the crystallization of the UiO-66 MOF which leads to the formation of defects by missing

connections of the benzenedicarboxylate ligands to Zr nodes or linker dislocation (Ragon et al., 2014).

The produced defects depend on the synthesis conditions used and they can be of two types. The first type of introduced defects corresponds to “missing linker defects”, the second type of defects corresponds to “missing node defects”. Additionally, the use of HCl for the introduction of defects may add charge-compensating chloride ions into the nodes of the UiO-66 framework. This added chloride ions may also affect the crystal properties of the material (Shearer et al., 2014).

1.5. Gas chromatography

1.5.1. Application of gas chromatography to the study of adsorptive desulfurization of liquid fuels

Gas chromatography has been used in the investigation of adsorptive desulfurization of liquid fuels. This technique has been used to monitoring the sulfur content of the fuel after treatment and for quantifying the sulfur concentration of individual sulfur compounds when the analyzed fuel is a model fuel as in the work by Ma and coworkers (Ma, Velu, Kim, & Song, 2005). Gas chromatography coupled to a sulfur specific detector is very useful for monitoring the changes in the sulfur matrixes of treated fuels, which means that the technique gives good information regarding any new sulfur compounds that may be created as a result of the desulfurization process. Among the most common detectors for sulfur detection in

gas chromatography are; Flame Photometric Detector (FID), Pulsed Flame Photometric Detector (PFPD), Atomic Emission Detector (AED), Sulfur Chemiluminescence Detector (SCD).

A major problem for the quantification of concentration of individual sulfur compounds in real fuels such as gasoline, diesel, or jet fuel, is the complex matrix of these fuels. Each fuel sample contains hundreds of sulfur compounds and hydrocarbons that may elute from the chromatographic column at similar times making the separation process a challenge. As shown in the work by Ma and coworkers, GC-FPD and GC-PFPD are not suitable for quantitative estimation of total sulfur concentration of gasoline samples without considering the nonlinear response of both detectors and the quenching effect in the fuel matrix (Ma et al., 2005). The quenching problem has also been reported in the work by Chambers and Duffy, who presented a detailed description of the PFPD detector with several applications using this detector for analyzing petrochemical samples (O.I. Analytical, 2007).

1.5.2. Pulsed Flame Photometric Detector (PFPD)

PFPD stands for Pulsed Flame Photometric Detector. Figure 1.5.2-1 shows the schematic of the model 5380 PFPD which is the one used in this work. The detector consists of a base, body, and a cap. The detector base connects the gas inlets and chromatography column end to the detector body. The detector body houses the combustor where the combustion of the sample happens. The combustor is filled with the sample and the combustor gas which is a mixture of air and

hydrogen in excess. The combustor wall is surrounded by a second mixture of hydrogen and air in excess. The detector cap houses the ignitor that starts the combustion, and it also has a vent for the exhaust gases.

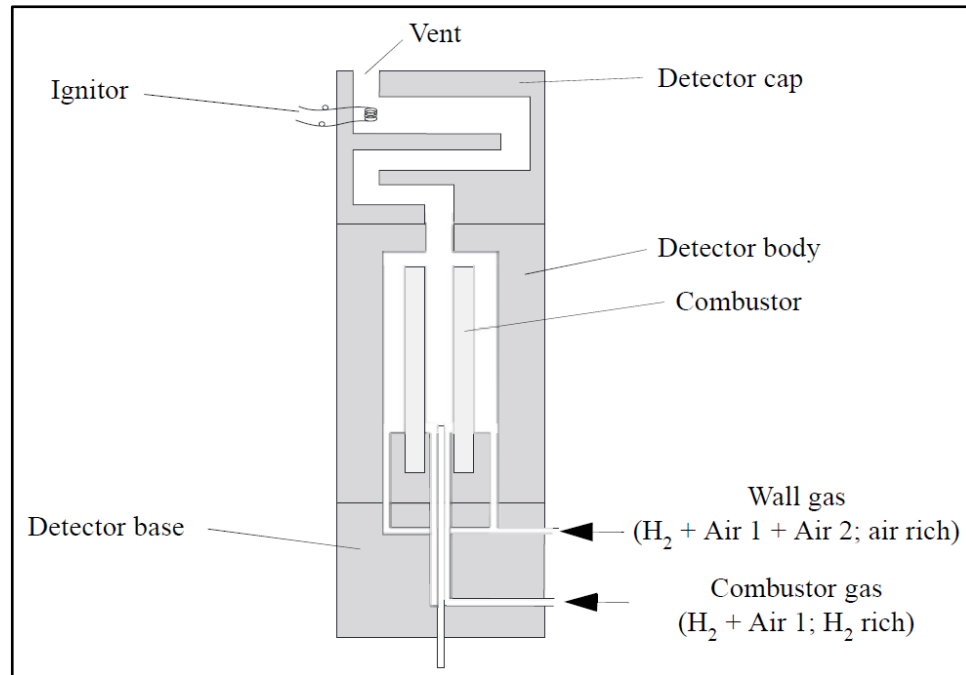


Figure 1.5.2-1. Combustor design and wall gas pathways (O.I. Analytical, 2004).

The PFPD works by a flame that is consumed in a fused silica tube known as Combustor. This combustion emits light with luminescent spectra and lifetime specific to each of the compounds present in the gas sample (O.I. Analytical, 2004).

The two combustion flows in the detector are used as follows; the first or primary flow is known as COMBUSTOR gas and it is the mixture of air and hydrogen (hydrogen rich) that meets the sample gas inside the combustor. The second or secondary flow is known as WALL gas; the wall gas is a mixture of hydrogen and air,

but air rich. This wall gas flows around the combustor wall and towards the ignitor. The wall gas is air rich for an easier ignition.

The PFPD cycle starts with the combustor gases filling up the combustor. At the same time, the wall gases flow up to the ignitor and escape through the vent sweeping any exhaust gases out the detector. Now that the path from the ignitor to the combustor is filled with the combustible gas mixture, the flame starts as soon the combustible mixture reaches the glowing ignitor. This flame then propagates down to the combustor and finishes towards its bottom. If the combustor gas is set correctly (GC effluent + air + hydrogen in excess), the flame should propagate towards the bottom of the combustor and extinguish after all the combustor gas is fully consumed (O.I. Analytical, 2004). A schematic of this cycle is shown in Figure 1.5.2-2.

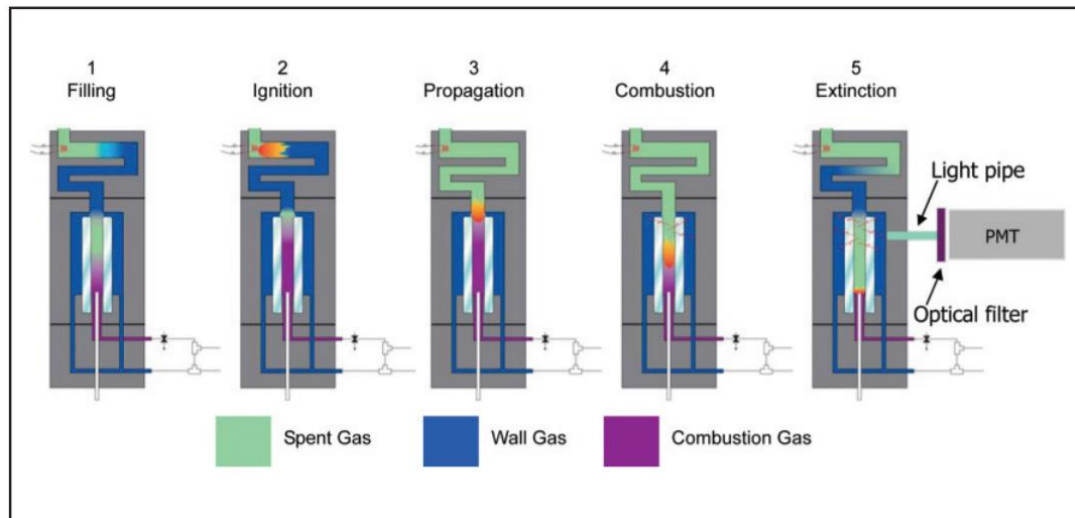


Figure 1.5.2-2. PFPD flame cycle (O.I. Analytical, 2004).

The PFPD is an improved version of a Flame Photometric Detector (FPD). But the PFPD is a pulsed detector which means it generates pulsed chemiluminescence. One of the most interesting features of the PFPD is its gated integration which allows it to reject all the undesired signal from the combustion of other elements. For example, the combustion of a hydrogen rich flame produces CH^* , C_2^* , and OH^* species. The emission lifetime depends on the combusted element; therefore, as shown in Figure 1.5.2-3, carbon and sulfur have different emissions lifetimes. Carbon emission lifetime ends before 3 milliseconds (ms), sulfur emission only reaches its maximum up to 6 ms after ignition and it can expand up to 24 ms. Thus, sulfur emission has chemiluminescent lifetime considerably longer than carbon emission. This chemiluminescent lifetime difference is exploited by using a gated integrator. Before using the detector, the operator can specify the time gate of the element of interest for the analysis. The gate for sulfur emission is 6 – 24 ms, therefore, when the detector is used in sulfur mode only the light emissions generated after 6 ms are considered as valid and detected. The light emission generated before 6 ms is ignored and does not contribute to the detected signal.

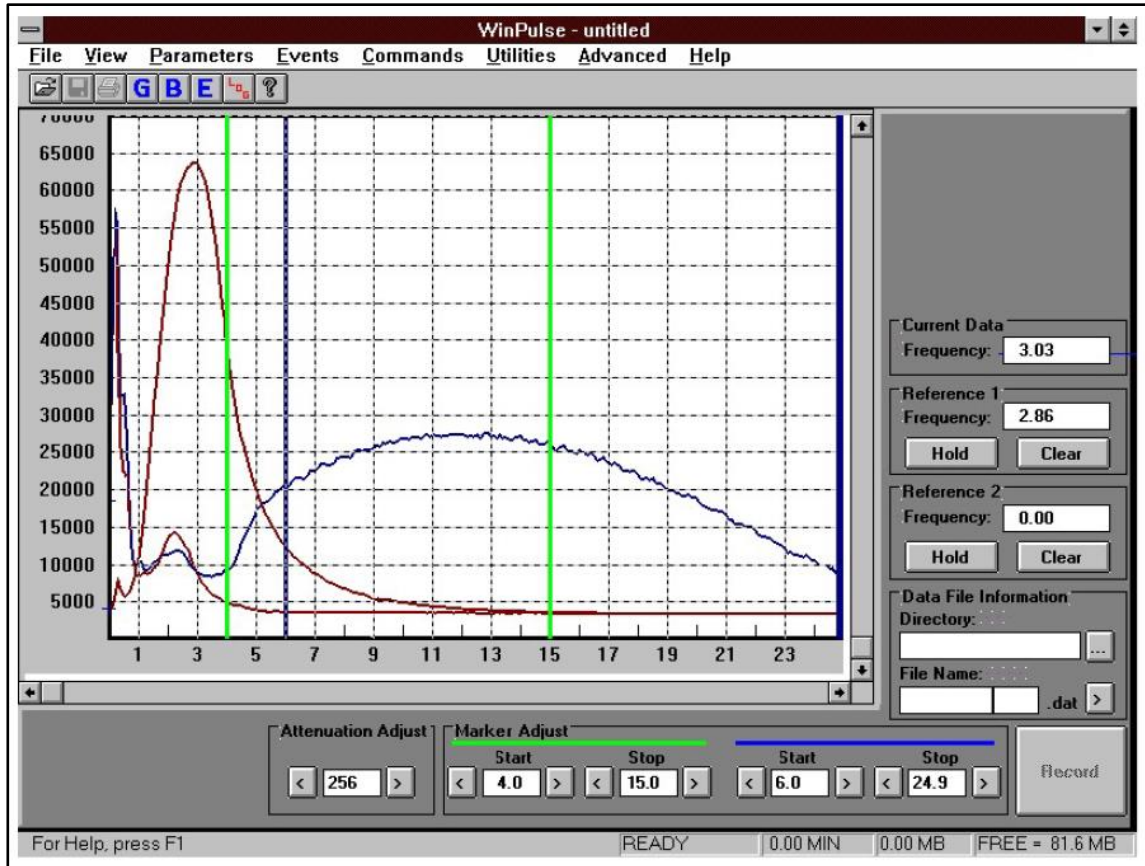


Figure 1.5.2-3. Lifetimes of carbon, phosphorus, and sulfur emissions (O.I. Analytical, 2004).

Some of the features of the model 5380 PFPD over its antecessor the FPD are;

- ✓ No need of sample concentration because the PFPD's improved sensitivity compared to that of the FPD. The PFPD can detect trace-level contaminants.
- ✓ Due to the dual gate capabilities, the detector shows a good selectivity of up to 28 different elements.
- ✓ Having a pulsed flame allows for constant reignition and avoids 'flameout' problems that can be a related to water or excess of solvent

in the gas flow. This was a typical problem in the FPD which works with a constant flame.

1.6. Research objectives

The aim of this thesis is to use gas chromatography to study the selective adsorptive desulfurization of JP-8 using CuNa-Y zeolite and defective UiO-66 metal-organic framework. The first question to answer is whether the sulfur removal by CuNa-Y zeolite is specific to a certain fraction of sulfur compounds in the matrix of JP-8, or if the removal is the same for the entire sulfur matrix. To answer this, the second chapter of this thesis presents the results of the batch adsorptive desulfurization experiments done on JP-8 samples which later are recovered and analyzed using Gas Chromatography coupled to a Pulsed Flame Photometric Detector (GC-PFPD), which is specific to sulfur compounds. The resulted chromatograms gave evidence of the sulfur compounds that are removed at the first stage of the process. After that, sequential desulfurization steps were performed to determine if CuNa-Y zeolite was able to remove all the sulfur compounds in the JP-8 matrix.

A second question surged regarding the adsorptive desulfurization performance of CuNa-Y zeolite. Knowing that the adsorbent could have both Cu(I) and Cu(II) cations on its structure, it is important to determine which is the role of each type of cation in the adsorptive desulfurization process. The results related to this question are presented in the third chapter of this thesis. This part of the work

consisted in the preparation of two adsorbents which then were calcined at different environments. One of the adsorbents was calcined under hydrogen (to increase the amount of Cu(I) cations), and the second one was calcined under dry air (to increase the amount of Cu(II) cations). Each adsorbent was used in desulfurization experiments and then the treated fuel samples were also analyzed by GC-PFPD. The quantification of the copper species in each zeolite sample was done by H_2 -TPR.

After studying the use of CuNa-Y zeolite as adsorbent for desulfurization of JP-8, a new kind of adsorbents were tested. Defective UiO-66 metal-organic framework adsorbents were synthesized and used to desulfurize JP-8 samples. The aim was to investigate whether the inclusion of defects in the structure of the UiO-66 metal-organic framework adsorbent could make a positive impact on the desulfurization performance of this material. The creation of defects would result in an adsorbent with bigger pores than those in CuNa-Y zeolite; therefore, we should expect that the bulkier sulfur compounds such as multiple-alkylated benzothiophenes would be removed easily. The results regarding this part of the work are presented in the fourth chapter of this thesis.

A fifth chapter is included which summarizes the main conclusions of this work as well as the proposed future work.

Gas chromatography study of the adsorptive desulfurization of JP-8 using CuNa-Y zeolite

2.1. Description

Zeolitic materials have been used as effective adsorbents for adsorptive desulfurization, being zeolite Y one of the most used materials for its stability, high surface area, and pore diameter. Besides, zeolite Y can be modified by ion exchange to add metal cations to its structure which are more selective to sulfur molecules resulting in a higher sulfur removal by the metal-loaded zeolite.

According to the work by Priscilla Dias da Silva and coworkers (Dias da Silva et al., 2019), adsorptive desulfurization of JP-8 at elevated temperatures enhances the sulfur removal, although which is the effect of temperature over the process is

still unknown. The higher sulfur removal may be a result of a higher selectivity of the adsorbent towards sulfur compounds caused by the increased temperature.

This chapter presents the adsorptive desulfurization of JP-8 using CuNa-Y zeolite and Na-Y zeolite for comparison. The experiments were done at 30°C, 80°C, 130°C, and 180°C, leaving the fuel in contact with the adsorbent for 6 hours. Then, the material was recovered through vacuum filtration, and the fuel samples were tested for measuring their total sulfur concentration using an X-ray Fluorescence analyzer, Sindie 7039 by XOS. Gas Chromatography coupled to Pulsed Flame Photometric Detector (GC-PFPD) was used to analyze the treated fuel samples and to determine any change in the JP-8 sulfur matrix due to the treatment. The objectives here are the following:

- ✓ To determine whether the desulfurization process using both zeolites produces any change in the sulfur matrix of the fuel.
- ✓ To investigate if CuNa-Y zeolite is more selective to a specific fraction of sulfur compounds in JP-8.

2.2. Experimental work

2.2.1. Preparation of zeolitic materials

Na-Y and CuNa-Y zeolite were used in this work. Na-Y zeolite was the pattern zeolite over which the copper cations were loaded through liquid metal ion exchange.

Na-Y zeolite was purchased from Alfa Aesar, powder form, Si/Al = 2.55. (add lot number). The material was mixed with deionized water and stirred for 24 hours at 300 rpm (revolutions per minute). After that, the zeolite was recovered through vacuum filtration and dried at 105°C for 24 hours. The dried material was then calcined under helium in a furnace with a temperature ramp of 10°C/min up to 450°C and kept at this temperature for 3 hours. After the calcination procedure, the activated zeolite was stored in a glass vial inside a desiccator.

CuNa-Y zeolite was prepared as follows; Na-Y zeolite was loaded with copper ions by liquid ion-exchange in aqueous copper nitrate, $\text{Cu}(\text{NO}_3)_2$. 28.1 g of copper nitrate were diluted in 150 mL of deionized water (DI water). After all solid were dissolved, 9.0 g of Y zeolite were added, and the mix was adjusted to 230 mL with DI water. Then, the mix was stirred for 24 hours at 300 rpm. After 24 hours, the solid material was recovered by vacuum filtration. The precipitate was washed with DI water and more DI water was added to adjust the mix to 230 mL. The mix was stirred for 2-3 minutes and then filtered again as before. The filter paper with the recovered solids were dried on a hot plate for 15-20 min at 150°C. After drying, the solids were put on a petri-dish and located into an oven at 105°C to let them dry for 24 hours. Before the desulfurization experiments, the CuNa-Y zeolite was activated by calcination in a furnace under helium using a temperature ramp of 10°C/min up to 450°C and keeping this temperature for 3 hours. The activated material was stored in a desiccator to avoid contact with humidity.

2.2.2. Characterization of Na-Y and CuNa-Y zeolites: XRD patterns

Powder X-ray diffraction (XRD) measurements of Na-Y and CuNa-Y zeolite were performed to confirm that the crystalline structure of the materials was kept after their preparation. The measurements were performed in a Rigaku D/Max (EAST) Ultima II diffractometer, using Cu-K α radiation. The 2θ measurement range was 3 - 50°. The measured patterns were then compared to the simulated pattern of Na-Y zeolite. The simulated pattern was obtained using the software Mercury 3.10.3 provided by The Cambridge Crystallographic Data Centre (CCDC).

The procedure for the preparation of these zeolites was taken from the work by Gupta and coworkers (Patent No. WO2017100617A1, 2016). Thus, the values of surface area and total metal content for each zeolite are also reported from that work. Gupta and coworkers reported that the total metal content was determined by ICP-OES (Optima 8300, Perkin Elmer), and the surface area was measured using a BET Surface Analyzer (Autosorb-iQ-MP/Kr, Quantachrome).

2.2.3. Preparation of fuel samples: JP-8

Jet fuel was used as received; the fuel was supplied by Synovision Solutions LLC in November 2017. The total sulfur concentration of this fuel was 2230 ppmw_S, measured by XRF.

2.2.4. Batch desulfurization of jet fuel at elevated temperatures

The desulfurization experiments were done in 125 mL PTFE liners and stainless-steel vessels (Parr Instruments). 20 mL of jet fuel were transferred to the

liner and then 200 mg of the adsorbent were added. The liner was covered with its cap and located into a stainless-steel vessel. Next, the vessel was closed tightly and secured with 8 bolts. Each vessel was located into an oven set at the desired temperature, 30°C, 80°C, 130°C, or 180°C, for 6 hours.

After 6 hours, the oven temperature was set to 25°C and the adsorbent material was recovered through vacuum filtration using a 0.2 μm filter. The treated fuel was stored in a glass vial. The wet adsorbent was put to dry on a petri dish for 24 hours. Then, the dry adsorbent was collected into a glass vial.

2.2.5. Total sulfur content measurement

Each treated jet fuel sample was tested by X-ray Fluorescence (XRF) to measure its total sulfur content. The measurements were done in an XRF sulfur analyzer, Sindie 7039 manufactured by X-Ray Optical Systems (XOS). The calibration curve was prepared using XOS sulfur standards in mineral oil with concentrations from 0 to 3000 ppmw of sulfur.

Equation 1. was used to calculate the amount of sulfur removed by each desulfurization experiment.

$$q_{S_{rem}} = (C_0 - C_f) \cdot \frac{V}{W}$$

Equation 2.2.5-1. Amount of sulfur removed (Dias da Silva et al., 2019)

Where,

$q_{S_{rem}}$; amount of sulfur removed (mg_S/g_ads)

C_0 ; initial sulfur concentration (mg_S/L)

C_f ; final sulfur concentration (mg_S/L)

V; total volume of treated fuel sample (L)

W; weight of adsorbent used per experiment (g)

2.2.6. GC-PFPD test of treated JP-8 samples

Gas Chromatography was used to analyzing the treated jet fuel samples to investigate for any change in their sulfur matrix. The system consisted of a gas chromatographer, Agilent 6890N series, coupled to a Pulsed Flame Photometric Detector (PDPF), model 5380 by OI Analytical, which is specific to sulfur. The gas chromatography system was configured with the characteristics listed in Table 2.2.6-1.

Table 2.2.6-1. GC-PFPD system description

Characteristic	Description
Inlet temperature	275 °C
Syringe capacity	5.0 μ L, autosampler injection
Injection volume	0.1 μ L

Column	Agilent, DB-1, non-polar, 7-inch cage Length: 60.0 m Internal diameter: 0.25 mm Film thickness: 1.00 μm Stationary phase: 100% Dimethylpolysiloxane
Mobile phase, carrier	Hydrogen; Ultra-high purity (UHP), Airgas 80 psig, 99.999% purity or better
Temperature program	35 $^{\circ}\text{C}$, hold for 6 min Raise to 170 $^{\circ}\text{C}$, 10 $^{\circ}\text{C}/\text{min}$ Raise to 228 $^{\circ}\text{C}$, 3 $^{\circ}\text{C}/\text{min}$ 228 $^{\circ}\text{C}$, hold for 2 min
Detector	Pulsed Flame Photometric Detector (PFPD), model 5380, manufactured by OI Analytical
Detector temperature	250 $^{\circ}\text{C}$
Combustor	2 mm diameter, sulfur mode
Combustion gases	Hydrogen; Ultra-high purity (UHP), Airgas, 60

	psig, 99.999% purity or better
	Air; Zero air, Airgas, 60 psig, 99.999% purity or better
Optical filter	BG-12 (purple)

The GC-PFPD method differs from the one used by Priscilla Dias da Silva and coworkers (Dias da Silva et al., 2019) by the type of column used, the temperature ramp, and the carrier selected. In this work, a slower temperature ramp was used to get a better separation of the sulfur compounds.

Several model sulfur compounds were tested using the GC-PFPD system to determine if any of those matched with the sulfur compounds in the matrix of JP-8.

2.2.7. Desulfurization of jet fuel by several desulfurization steps at 180°C

From the work by Priscilla Dias da Silva and coworkers (Dias da Silva et al., 2019), it is known that 180°C is the temperature at which the highest sulfur removal from JP-8 is achieved by CuNa-Y zeolite. Therefore, a series of desulfurization steps was done to determine the maximum sulfur removal this adsorbent can reach by consecutive steps. The desulfurization process was the same as explained in section 2.2.4. The only difference in the process was that CuNa-Y zeolite pellets were used instead of the powder form of the adsorbent. This modification was applied due to

the large amount of adsorbent needed to complete the process. For the first two desulfurization steps (A and B), the amount of 0.025 g-adsorbent/mL-fuel was used. The following two steps (C and D) were performed with 0.05 g-adsorbent/mL-fuel. The last two steps were performed with double the amount of adsorbent than for steps A and B to compensate the lower adsorption driving force caused by the decreased sulfur concentration of the fuel. The pellets were ordered from Riogen Inc. As before, liquid ion-exchange was used to load the pellets with copper ions; the liquid ion-exchange details are presented in section 2.2.1. The pellets contained a 20% of alumina binder and their total copper content was 6.9%. The shape of the pellets was cylindrical with 1.6mm of diameter and length between 2 and 10mm. This work was done in collaboration with Pricilla Dias da Silva and the results have been reported in (Dias da Silva et al., 2019).

2.3. Description of results and analysis

2.3.1. Characterization of Na-Y and CuNa-Y zeolites: XRD patterns

The experimental XRD patterns of Na-Y and CuNa-Y zeolites are presented in Figure 2.3.1-1. The simulated pattern for Na-Y zeolite is also shown for comparison. Both patterns for Na-Y and CuNa-Y zeolites are very similar to the simulated pattern for Na-Y zeolite, this indicates the zeolites kept the crystalline structure of the pristine Na-Y zeolite after their preparation.

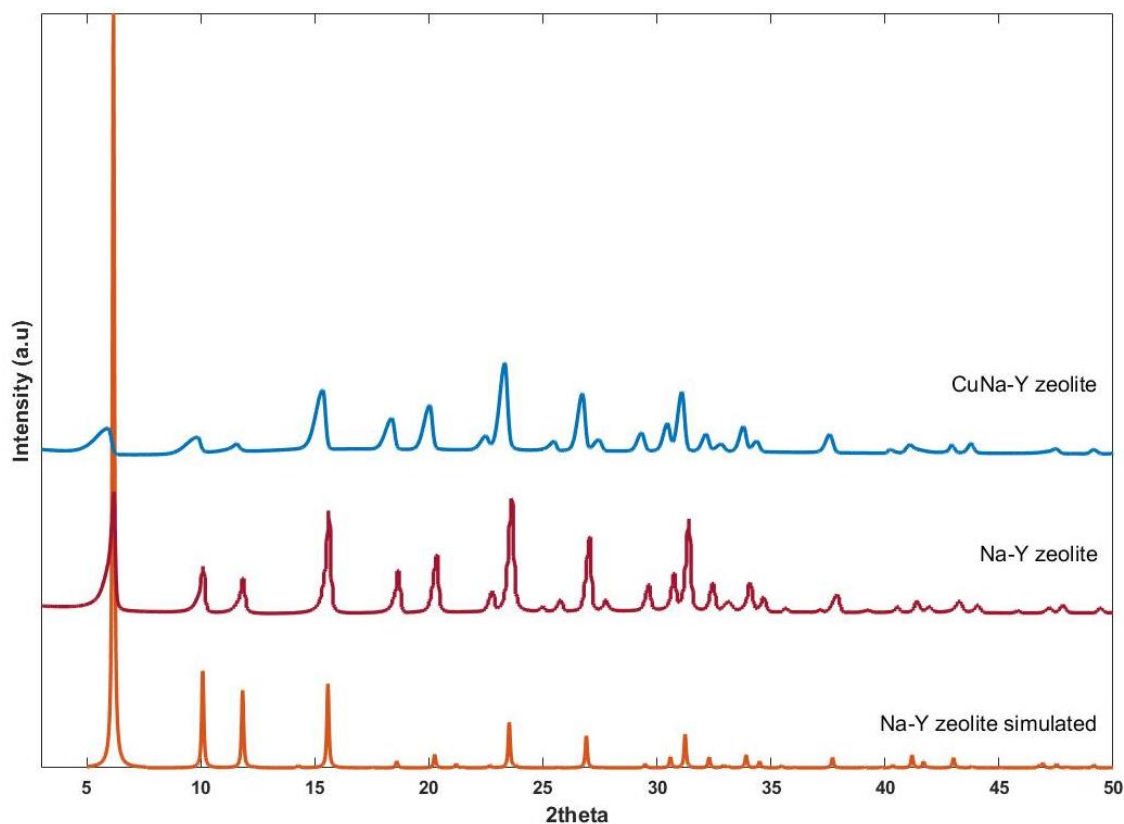


Figure 2.3.1-1. Experimental and simulated XRD patterns for Na-Y and CuNa-Y zeolites.

The results of surface area and metal content were taken from the work by Gupta and coworkers (Patent No. WO2017100617A1, 2016); those results are presented in Table 2.3.1-1. Comparing the values of surface area between Na-Y and CuNa-Y zeolites, it is seen that even after the metal ion exchange that adds copper cations to the Na-Y zeolite, its surface area remained almost the same.

Table 2.3.1-1. Properties of zeolitic adsorbents (Patent No. WO2017100617A1, 2016)

Adsorbent	Surface Area ($\frac{m^2}{g}$)	Total Metal content (%wt)	Metal sites distribution	Pore diameter (nm)
Na-Y zeolite	650	Na: 12.4 %wt	100 %Na	0.8 – 1.2
CuNa-Y zeolite	623	Cu: 8.2 %wt	46 %Cu; 54 %Na	0.8 – 1.2

2.3.2. Batch desulfurization of jet fuel at elevated temperatures

The batch desulfurization experiments were performed at 30°C, 80°C, 130°C, and 180°C. These experiments were done in collaboration with Priscilla Dias da Silva, and the results were taken from (Dias da Silva et al., 2019).

The pristine Na-Y zeolite was not effective to remove considerable amounts of sulfur from JP-8 at any of the tested temperatures. On the other hand, CuNa-Y zeolite performed better, showing a higher sulfur removal as temperature increases. The maximum sulfur removal was reached at 180°C with 36 mg_S/g_{adsorbent} compared to the 2.5 mg_S/g_{adsorbent} removed at 30°C. The results of sulfur removal by each zeolite at the four temperatures are displayed in Figure 2.3.2-1.

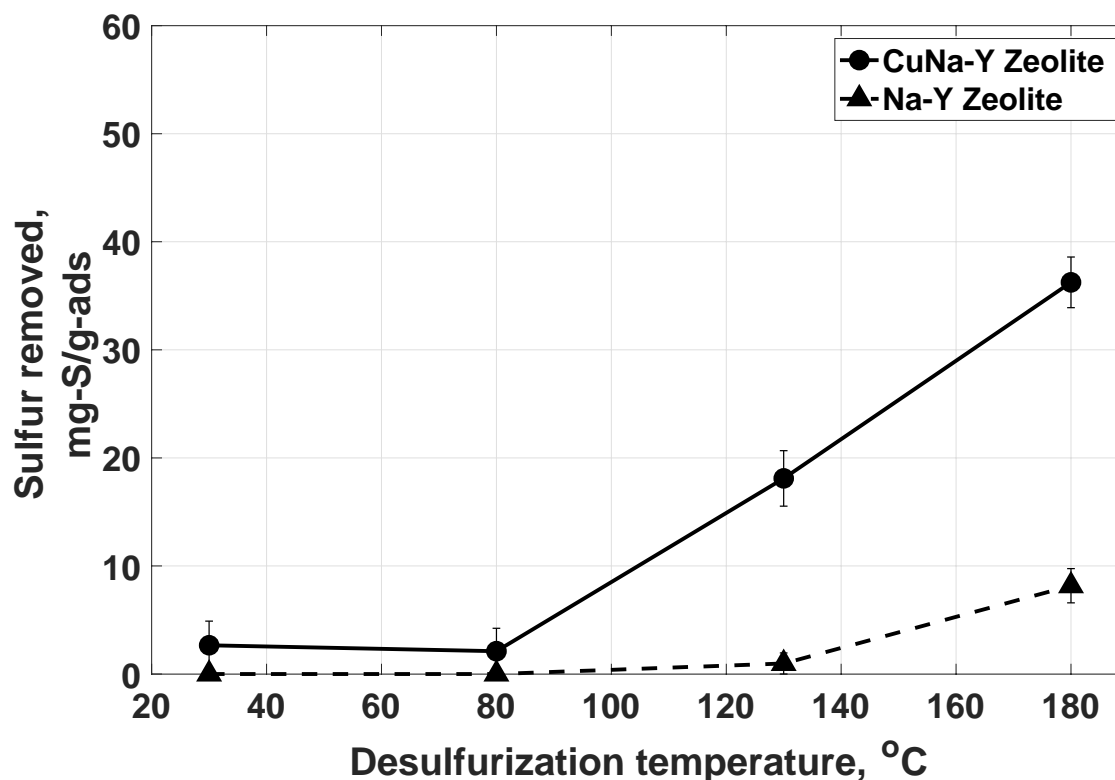


Figure 2.3.2-1. Total sulfur removed from JP-8 at 30°C, 80°C, 130°C, and 180°C by CuNa-Y and Na-Y zeolites. Initial sulfur concentration of JP-8 was 2230 ppmw_S. Retrieved data from: (Dias da Silva et al., 2019).

The competition among aromatic compounds and sulfur compounds present in JP-8 may be the reason for Na-Y zeolite to not remove sulfur molecules from JP-8. Regarding CuNa-Y zeolite, it has similar surface area as Na-Y zeolite, and their zeolitic frameworks are the same. Thus, it must be the presence of the copper cations in CuNa-Y zeolite which improves the selectivity of CuNa-Y towards sulfur compounds at 30°C and 80°C. As the work temperature increases (130°C and 180°C), the sulfur removal is considerably higher than that achieved by Na-Y zeolite at both temperatures. Therefore, the elevated temperature has a positive effect on the sulfur removal from JP-8. As reported by Priscilla Dias da Silva and coworkers

(Dias da Silva et al., 2019), the higher sulfur removal by CuNa-Y zeolite at elevated temperatures may be the result of a more specific sulfur-metal bond (between sulfur and the copper cations on the zeolite) that is activated as the temperature of work increases. This means that the interaction between copper cations and the sulfur molecules present in JP-8 is stronger than the interaction of the same cations with other molecules such as the aromatics that are also present in the fuel.

2.3.3. GC-PFPD test of treated JP-8 samples

First, the signal from different model sulfur compounds tested with the GC-PFPD system is presented. The signal from all compounds was compared to the signal from the sulfur compounds present in JP-8. The chromatograms are shown in Figure 2.3.3-1. As can be seen in Figure 2.3.3-1, the sulfur compounds found in JP-8 are close in retention times to the signal from the sulfur standards of benzothiophene and 3-methylbenzothiophene. This observation agrees with the results reported in the literature indicating that the main sulfur compounds present in jet fuel samples are benzothiophene and alkyl-benzothiophenes such as 2,3-dimethylbenzothiophene and 2,3,7-trimethylbenzothiophene (Link et al., 2003), (Lee & Ubanyionwu, 2008).

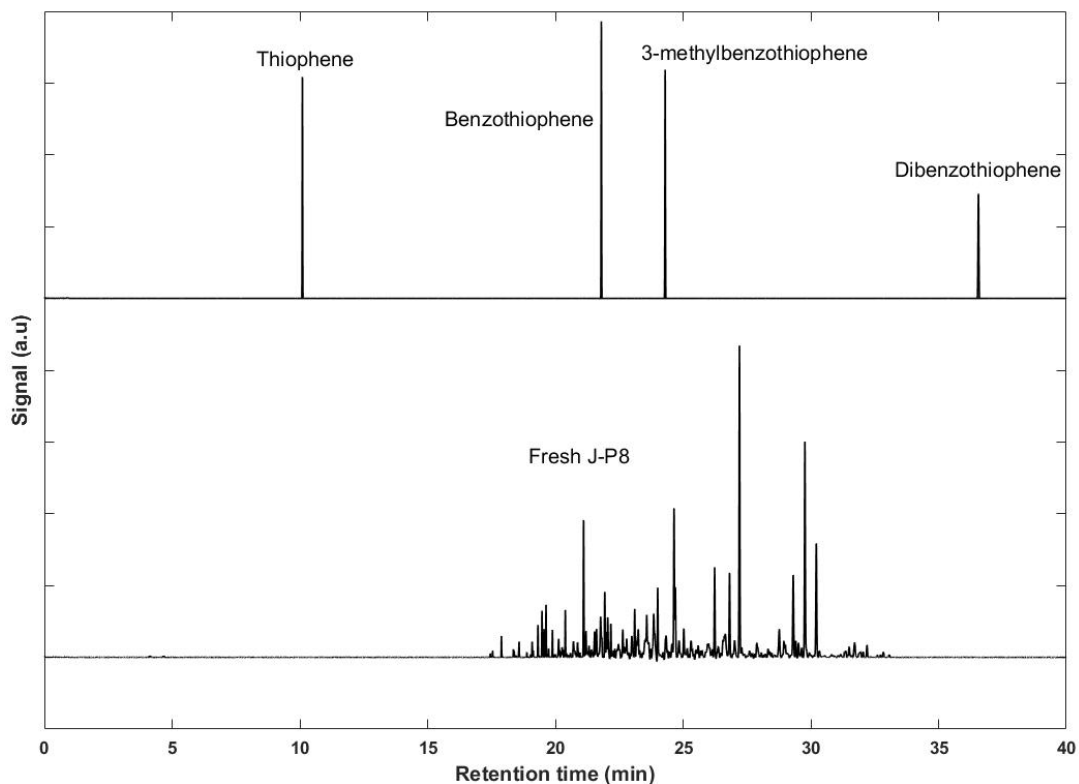


Figure 2.3.3-1. Gas chromatograms (pulsed flame photometric detection) of thiophene, benzothiophene, 3-methylbenzothiophene, and dibenzothiophene (top) and chromatogram of sulfur compounds present in fresh JP-8 (bottom). The concentration of the thiophene, benzothiophene, 3-methylbenzothiophene, and dibenzothiophene samples was 25 ppmw_S each. The samples were prepared diluting the pure model sulfur compound in iso-octane. The JP-8 samples was used as received, its concentration was 2230 ppmw_S. Retrieved data from: (Dias da Silva et al., 2019)

This section also presents the results of the GC-PFPD analysis of the JP-8 samples treated with Na-Y or CuNa-Y zeolite. First, Figure 2.3.3-2 shows the chromatograms for JP-8 without treatment, and for JP-8 treated with CuNa-Y zeolite at the four studied temperatures.

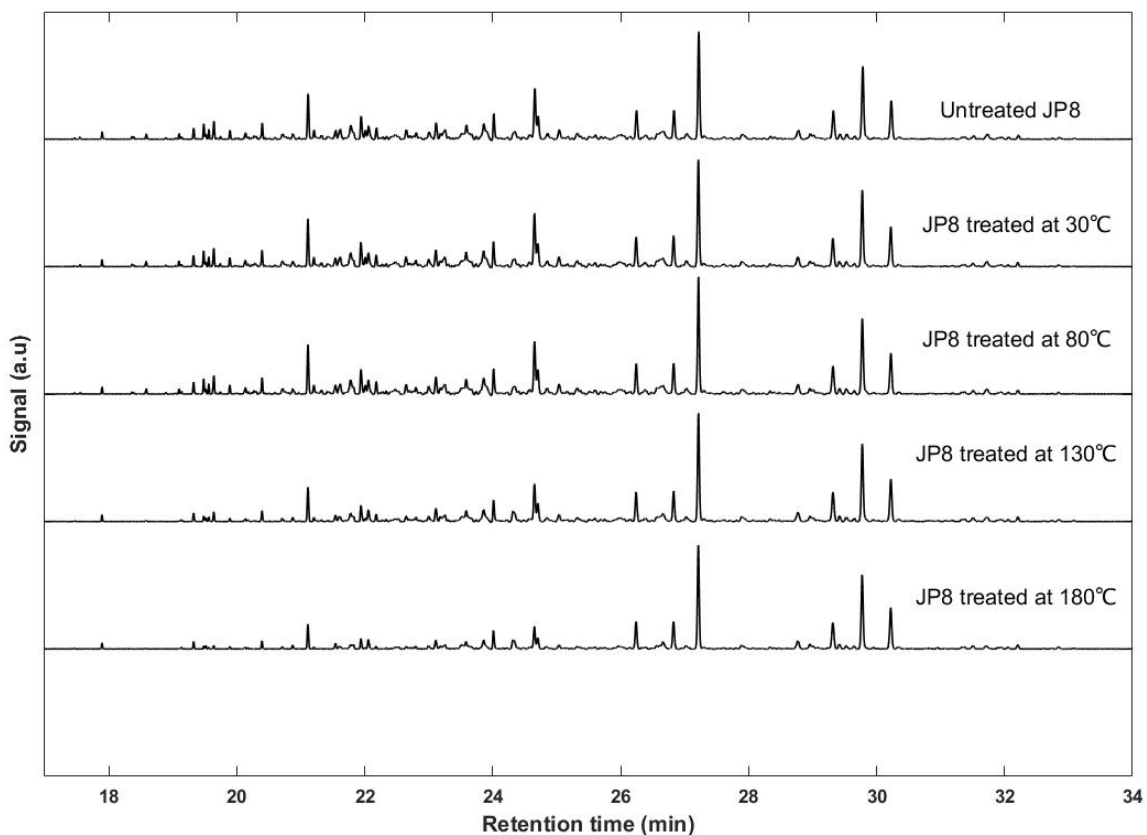


Figure 2.3.3-2. GC-PFPD results for JP-8 treated with CuNa-Y zeolite. From top to bottom: Untreated JP-8, JP-8 treated at 30°C, 80°C, 130°C, and 180°C. Retrieved data from: (Dias da Silva et al., 2019)

From the results shown in Figure 2.3.3-2, it can be seen that for the fraction of sulfur compounds from the retention times of 17 min to 25 min, the relative area of the peaks correspondent to that fraction decreases as temperature of treatment increases. Thus, the relative area of this fraction of sulfur compounds for the chromatogram of JP-8 treated at 180°C is considerably lower compared to that of untreated JP-8, or those of JP-8 treated at 30°C and 80°C.

For the GC-PDPF system used in this work, the lower the retention time in the chromatogram, the lighter the molar mass of the compound eluting at that retention time, and its boiling point is also lower. Therefore, the observation that CuNa-Y zeolite preferentially removed the sulfur compounds of lower molar mass and lower boiling point may indicate that this adsorbent is more selective towards the lighter sulfur compounds present in JP-8.

Comparing the chromatograms displayed in Figure 2.3.3-2, it can be seen that after treating the JP-8 with CuNa-Y zeolite, the sulfur matrix of the fuel did not change at any of the treatment temperatures. Therefore, the desulfurization process using CuNa-Y zeolite does not produce any new sulfur compounds.

The control experiments were done using Na-Y zeolite as the adsorbent material. Figure 2.3.3-3 shows the chromatograms for the untreated and treated (at the four temperatures) JP-8 samples. The sulfur matrix of jet fuel is preserved at each of the work temperatures, and the sulfur content seems not to have changed significantly in the samples treated at 30°C, and 80°C. But there was some sulfur removal from the jet fuel samples treated at 130°C and 180°C. The most appreciable difference is observed around the retention times 24 – 25 min, where there is a peak which area increases as the desulfurization temperature increases. This may be an indication of the formation of that specific sulfur compound because of a chemical reaction produced by the adsorbent material, or the formation of that compound as the desulfurization temperature is higher, or a combination of both.

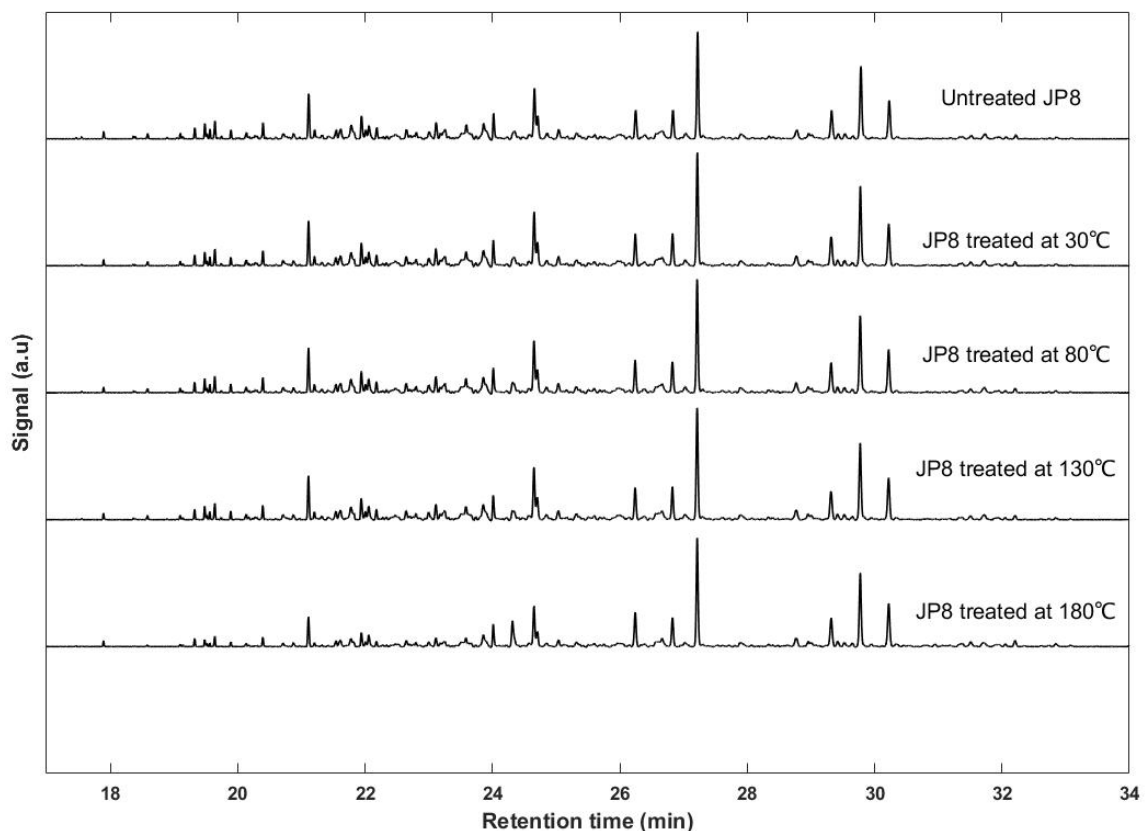


Figure 2.3.3-3. GC-PFPD results for JP-8 treated with Na-Y zeolite. From top to bottom: Untreated JP-8, JP-8 treated at 30°C, 80°C, 130°C, and 180°C. Retrieved data from: (Dias da Silva et al., 2019).

A set of experiments was done by only heating the fuel at the four temperatures but without any adsorbent. This was done to determine if the creation of the compound observed in Figure 2.3.3-3 between 24 – 25 min was a result of the desulfurization temperature. The chromatograms for the samples treated only by heating are displayed in Figure 2.3.3-4.

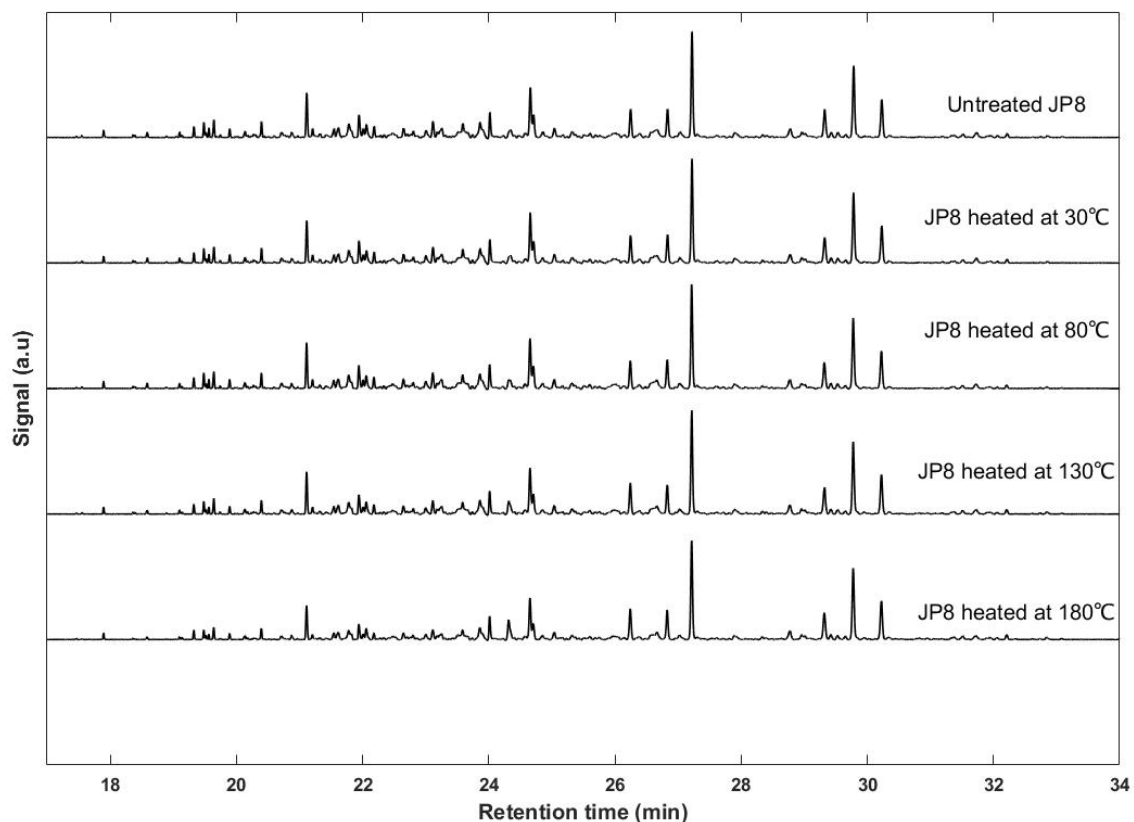


Figure 2.3.3-4. GC-PFPD results for JP-8 treated only by heating. From top to bottom: Untreated JP-8, JP-8 heated at 30°C, 80°C, 130°C, and 180°C. Retrieved data from: (Dias da Silva et al., 2019).

From Figure 2.3.3-4, effectively the peak area of the compound eluting between 24 – 25 min increases as the heating temperature increases. Therefore, the production of this compound is caused by heating the fuel and not by a reaction with the Na-Y zeolite. Going back to Figure 2.3.3-2 where the chromatograms for the fuel samples treated with CuNa-Y zeolite are shown, this peak shows no change at any temperature, which indicates that even though heating the fuel produces more of that compound, CuNa-Y zeolite is effective to remove it at the highest temperature.

2.3.4. Desulfurization of jet fuel by several desulfurization steps at 180°C

A series of four desulfurization steps was done over JP-8 using CuNa-Y zeolite pellets as adsorbent. The treated fuel samples were measured for total sulfur content by XRF. The samples were also tested by GC-PFPD to evaluate the changes on the sulfur matrix of the fuel after each desulfurization step. These results are shown in Figure 2.3.4-1.

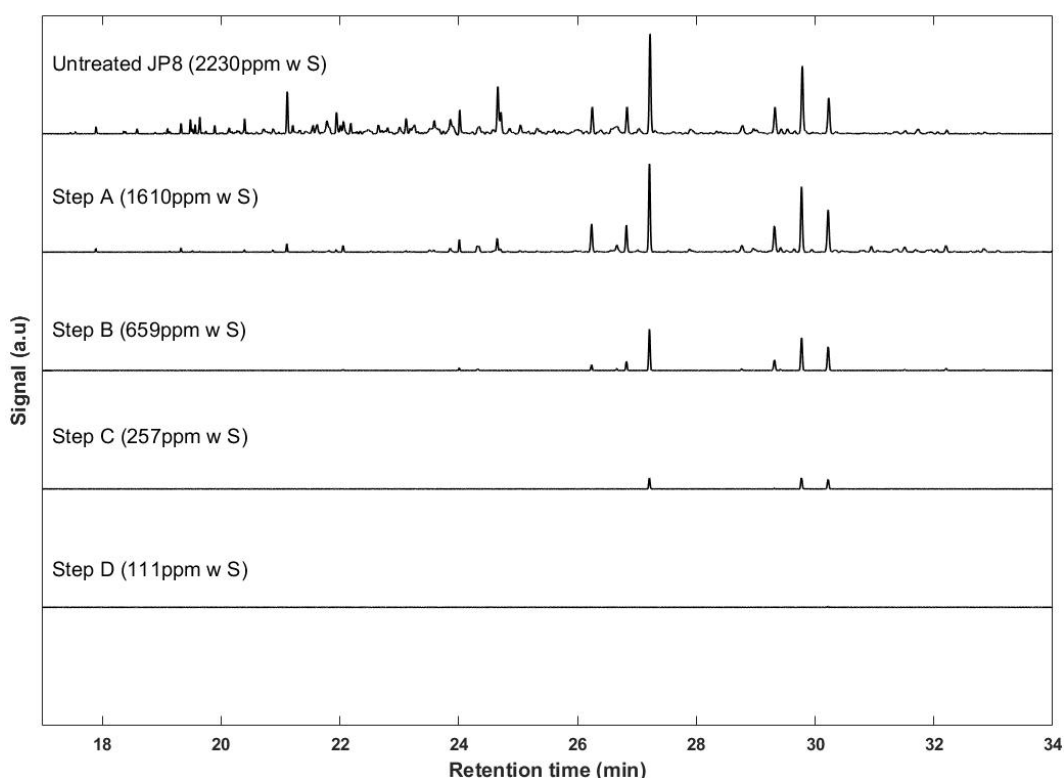


Figure 2.3.4-1. Chromatograms of JP-8 samples after four consecutive desulfurization steps. From top to bottom: Untreated JP-8, first to fourth desulfurization steps. CuNa-Y zeolite pellets were used as adsorbent material. The total sulfur content for each fuel sample was measured by XRF. Chromatograms were obtained by GC-PFPD. Retrieved data from: (Dias da Silva et al., 2019)

Figure 2.3.4-1 displays the chromatograms of the treated jet fuel samples after each desulfurization step. On top of the figure, the chromatogram of the untreated fuel is shown for comparison. Step A in Figure 2.3.4-1 shows that the desulfurization process removed first the lower boiling points sulfur compounds from JP-8. After the fuel was treated a second time (Step B), it is more evident that the process kept removing the lower boiling points sulfur compounds from JP-8. As the desulfurization steps moved forward (steps C and D), the CuNa-Y adsorbent removed also the higher boiling points sulfur compounds present in JP-8. The chromatogram of step D in Figure 2.3.4 1 looks flat as if there were no remaining sulfur compounds in the fuel, although after step D the fuel still had a sulfur content of 111 ppmw_S. The great decreasing in area of the chromatogram of the sample treated in step D (111 ppmw_S) compared to the chromatogram of the fresh JP-8 sample (2230 ppmw_S) agrees with the quadratic relationship between the sulfur concentration and the peak area produced by the PFPD. The quadratic response of the PFPD has been reported by the manufacturer and other researchers who are familiar with this detector (O.I. Analytical, 2004), (Amirav & Jing, 1995).

The sample treated in step D was analyzed again using an attenuation factor of 1 (10 times smaller than the attenuation factor used for the chromatograms in Figure 2.3.4-1). Using an attenuation factor of 1, the limit of detection of the system was less than 1 ppmw_S. The new chromatogram for step D is shown in Figure 2.3.4-2.

As shown in Figure 2.3.4-2, more sulfur compounds were detected by using an attenuation factor of 1 instead of 10. However, the newly observed sulfur compounds corresponded mostly to the higher boiling points sulfur compounds and this result agreed well with the observed desulfurization trend. Low boiling points sulfur compounds were removed first, and as the desulfurization steps continued, the higher boiling points sulfur compounds were also removed.

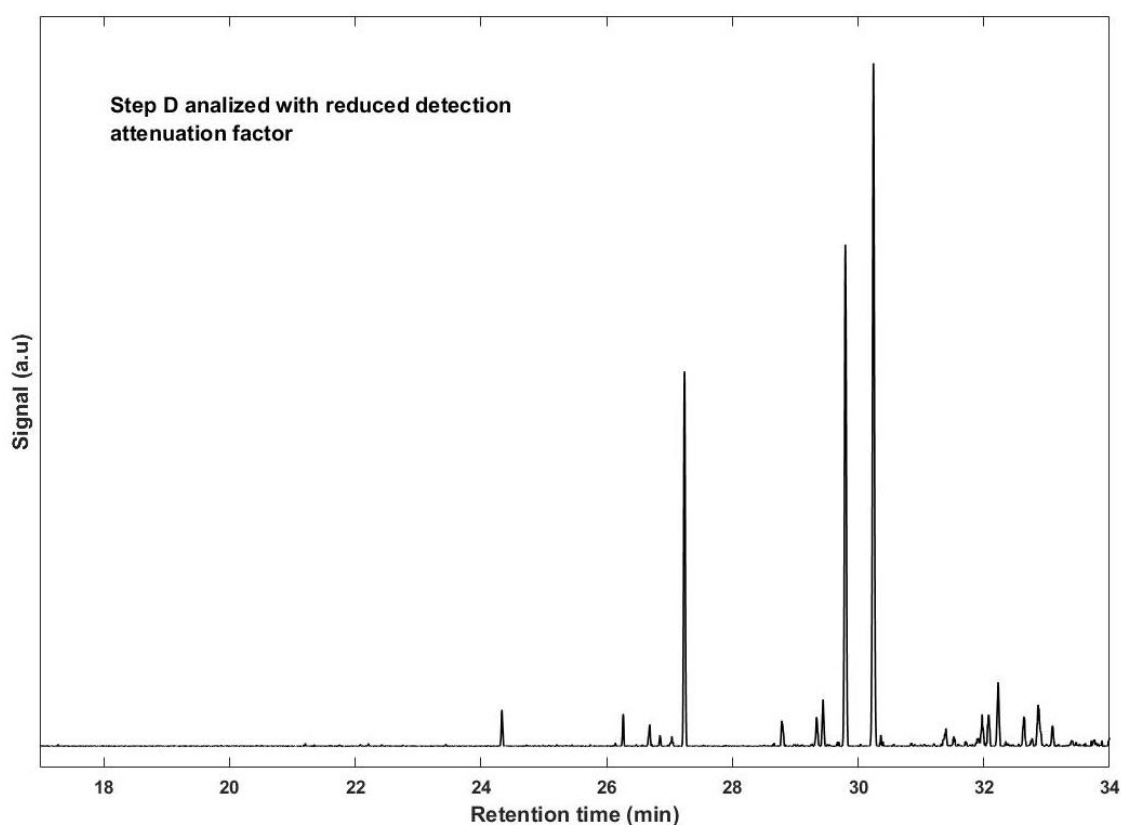


Figure 2.3.4-2. Step D in the series of four desulfurization steps of JP-8. CuNa-Y zeolite pellets were used as adsorbent material. The chromatogram was obtained by GC-PFPD using an attenuation factor of 1. Retrieved data from: (Dias da Silva et al., 2019)

The sequential desulfurization process demonstrated that even though the CuNa-Y zeolite adsorbent initially was more selective towards the fraction of lighter

sulfur compounds of JP-8, after several desulfurization steps the adsorbent removed all fractions of sulfur compounds effectively. These results show evidence of the opportunity of reaching ultra-low sulfur content in JP-8 by treating the fuel in a flow reactor at 180°C.

2.4. Conclusions

The analysis of the treated fuel samples by GC-PFPD showed that the adsorptive desulfurization of JP-8 using either Na-Y or CuNa-Y zeolites did not change the sulfur matrix of the fuel, which means the process only removed the sulfur molecules but not involved a chemical reaction between each of the zeolites and the fuel.

The approach of desulfurizing JP-8 by a series of four desulfurization steps proved the CuNa-Y zeolite can remove all fractions of sulfur compounds from JP-8. Certainly, the material first showed more selectivity towards the lighter sulfur compounds, but after the fourth desulfurization step, the material removed almost all sulfur compounds from JP-8. Based on these results, an effective strategy for producing ultra-low sulfur JP-8 may be to treat the fuel in a flow reactor unit at 180°C.

Study of the role of Copper species in adsorptive desulfurization using CuNa-Y zeolite

3.1. Introduction

After activation of CuNa-Y zeolite, copper cations may be as Cu(I) or Cu(II) oxidation states depending on the location of the cation in the zeolitic framework. To understand which the role of each type of cation in the desulfurization of JP-8 is two zeolites with a major content of each cation were prepared. Both zeolites were used to desulfurize JP-8 at four different temperatures. The treated fuel samples were analyzed by XRF and GC-PFPD.

3.2. Experimental work

3.2.1. Preparation of Cu(I)Na-Y and Cu(II)Na-Y zeolites

First, CuNa-Y zeolite was prepared as follows; Na-Y zeolite was loaded with copper ions by liquid ion-exchange in aqueous copper nitrate, $\text{Cu}(\text{NO}_3)_2$. 28.1 g of copper nitrate were diluted in 150 mL of deionized water (DI water). After all solid were dissolved, 9.0 g of Y zeolite were added, and the mix was adjusted to 230 mL with DI water. Then, the mix was stirred for 24 hours at 300 rpm. After 24 hours, the solid material was recovered by vacuum filtration. The precipitate was washed with DI water and more DI water was added to adjust the mix to 230 mL. The mix was stirred for 2-3 minutes and then filtered again as before. The filter paper with the recovered solids were dried on a hot plate for 15-20 min at 150°C. After drying, the solids were put on a petri-dish and located into an oven at 105°C to let them dry for 24 hours.

The type of copper cation present in the zeolite depends on the reduction environment used during the activation stage. Cu(I)Na-Y zeolite was prepared by calcining the regular CuNa-Y zeolite under hydrogen. Cu(II)Na-Y was prepared by calcination under dry air. The temperature ramp used for both zeolites was 10°C/min up to 450°C, keeping this final temperature for 3 hours. Cu(I)Na-Y zeolite was stored under argon gas; Cu(II)Na-Y zeolite was stored in a desiccator to avoid contact with humidity.

3.2.2. Characterization of Cu(I)Na-Y and Cu(II)Na-Y zeolites: XRD patterns and Hydrogen Temperature Programmed Reduction (H_2 -TPR) experiments

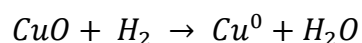
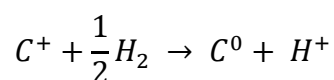
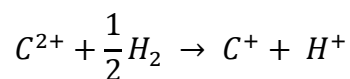
Powder X-ray diffraction (XRD) measurements of Cu(I)Na-Y and Cu(II)Na-Y zeolites were performed to confirm that the crystalline structure of the materials was kept after their preparation. The measurements were performed in a Rigaku D/Max (EAST) Ultima II diffractometer, using Cu-K α radiation. The 2θ measurement range was 3 - 50°. Because the copper cations in Cu(I)Na-Y are prone to oxidize back to Cu(II), and all the XRD measurements were done under ambient conditions, the XRD pattern for Cu(I)Na-Y zeolite will correspond to its reoxidized state.

The measured patterns were compared to the simulated pattern of Na-Y zeolite. The simulated pattern was obtained using the software Mercury 3.10.3 provided by The Cambridge Crystallographic Data Centre (CCDC).

Hydrogen Temperature Programmed Reduction (H_2 -TPR) experiments were performed to identify the type of copper cation present in each copper zeolite and for quantifying the total content of Cu(I) or Cu(II) in both zeolites. The TPR experiments were done using a Micromeritics Autochem II coupled with a thermal conductivity detector (TCD). Each H_2 -TPR experiment was conducted using 50 mg of CuNa-Y zeolite under $5 \frac{cm^3}{min}$ flow of 10.125%wt H_2 /Ar. The temperature ramp used for each analysis was 10 °C/min. The H_2 -TPR were performed both after ex-situ and in-situ activation of CuNa-Y zeolite under either hydrogen for Cu(I)Na-Y zeolite, or dry air for Cu(II)Na-Y zeolite. Ex-situ activation refers to the activation of

the zeolite in an external furnace; after the activation the zeolite sample was transported and analyzed in the Micromeritics Autochem II. In-situ activation refers to the activation of the zeolite sample already in the Micromeritics Autochem II previous its H_2 -TPR analysis. For the in-situ activation, the sample was heated from room temperature to 450°C at 10 °C/min, and the final temperature was kept for 30 min. Right after activation was done and the sample cooled down, the H_2 -TPR started in the same equipment. The H_2 -TPR results were used to determine the type and amount of copper cations present in each zeolite.

For the quantification of the copper species, the following reaction mechanism was considered, which correspond to the reduction of copper species under hydrogen as reducing agent.



Equation 3.2.2-1. Chemical mechanism for the reduction of copper species in CuNa-Y zeolite under hydrogen as reducing agent (Richter et al., 2007).

The reduction of Cu(II) to metallic copper (Cu^0) occurs in two steps. First, Cu(II) reduces to Cu(I) at temperature between 150 - 450°C. Second, Cu(I) reduces to Cu^0 at temperature between 800 - 900°C. The reduction of copper oxide (CuO) to

metallic copper (Cu^0) occurs at temperature between 180 - 285°C (Richter et al., 2007).

3.2.3. Preparation of fuel samples: Model fuels and JP-8

Model fuels were used for this part of the work; the solvent used was n-dodecane (Fisher Scientific) because is a good representant of the alkyl chains of more relevance in jet fuel (Bakshi & Henderson, 1998). The model sulfur compound used in model fuels was 3-methylbenzothiophene (3-MBT, Sigma Aldrich) in a concentration of 2000 ppmw of sulfur; the first model fuel will be referred as MF.

Another model fuel, also a dissolution of 3-MBT in n-dodecane (2000 ppmw of sulfur), includes toluene to mimic the aromatic content present in jet fuel; the total toluene content was 15%wt which is the approximate aromatic concentration in jet fuel. This second model fuel will be referred as MFT.

Real jet fuel was also tested to determine the effectiveness of each zeolite to remove sulfur from complex sulfur matrix. JP-8 was used as received from Synovision Solutions LLC in November 2017. The total sulfur concentration of this fuel was 2230 ppmw_S, measured by XRF.

The description of each fuel tested in this section is presented in Table 3.2.3-1.

Table 3.2.3-1. List of tested fuels

Name of fuel	Total Sulfur Content (ppmw)	Total Aromatic Content (%wt)
MF (3-MBT in n-dodecane)	≈ 2000	0 %wt
MFT (3-MBT in n-dodecane + toluene)	≈ 2000	≈ 15 %wt
JP-8 (used as received)	≈ 2230	≈ 15 %wt

3.2.4. Batch desulfurization of fuels at elevated temperatures

As explained in section 2.2.4, the desulfurization experiments were done in polyethylene liners and stainless-steel vessels. 20 mL of jet fuel were transferred to the liner and then 200 mg of the adsorbent were added. The liner was covered with its cap and located into a stainless-steel vessel. Next, the vessel was closed tightly and secured with 8 bolts. Each vessel was located into an oven set at the desired temperature, 30°C, 80°C, 130°C, or 180°C, for 6 hours.

After 6 hours, the oven temperature was set to 25°C and the adsorbent material was recovered through vacuum filtration. The treated fuel was stored in a glass vial. The wet adsorbent was put to dry on a petri dish for 24 hours. Then, the dry adsorbent was collected into a glass vial.

3.2.5. Total sulfur content measurement

Each jet fuel sample was tested by X-ray Fluorescence (XRF) to measure its total sulfur content. The measurements were done in an XRF sulfur analyzer, Sindie 7039 manufactured by X-Ray Optical Systems (XOS).

3.2.6. GC-PFPD test of treated JP-8 samples

Gas Chromatography was used to analyzing the treated jet fuel samples to investigate for any change in their sulfur matrix. The system consisted of a gas chromatographer, Agilent 6890N series, coupled to a Pulsed Flame Photometric Detector (PDPF), model 5380 by OI Analytical, which is specific to sulfur. A complete description of the gas chromatography system configuration is presented in Table 2.2.6-1.

3.3. Description of results and analysis

3.3.1. Characterization of Cu(I)Na-Y and Cu(II)Na-Y zeolites: XRD patterns and H_2 -TPR results

The XRD patterns of Cu(I)Na-Y and Cu(II)Na-Y zeolites are shown in Figure 3.3.1-1. The simulated pattern of the Na-Y is also shown for comparison. The XRD patterns were measured under ambient conditions therefore, the patterns for Cu(I)Na-Y zeolite correspond to a hydrated and re-oxidized state of the sample. Since the measured XRD patterns show all the characteristic peaks of Na-Y zeolite, it

is demonstrated that all the zeolitic materials kept their crystalline structure after their preparation and activation.

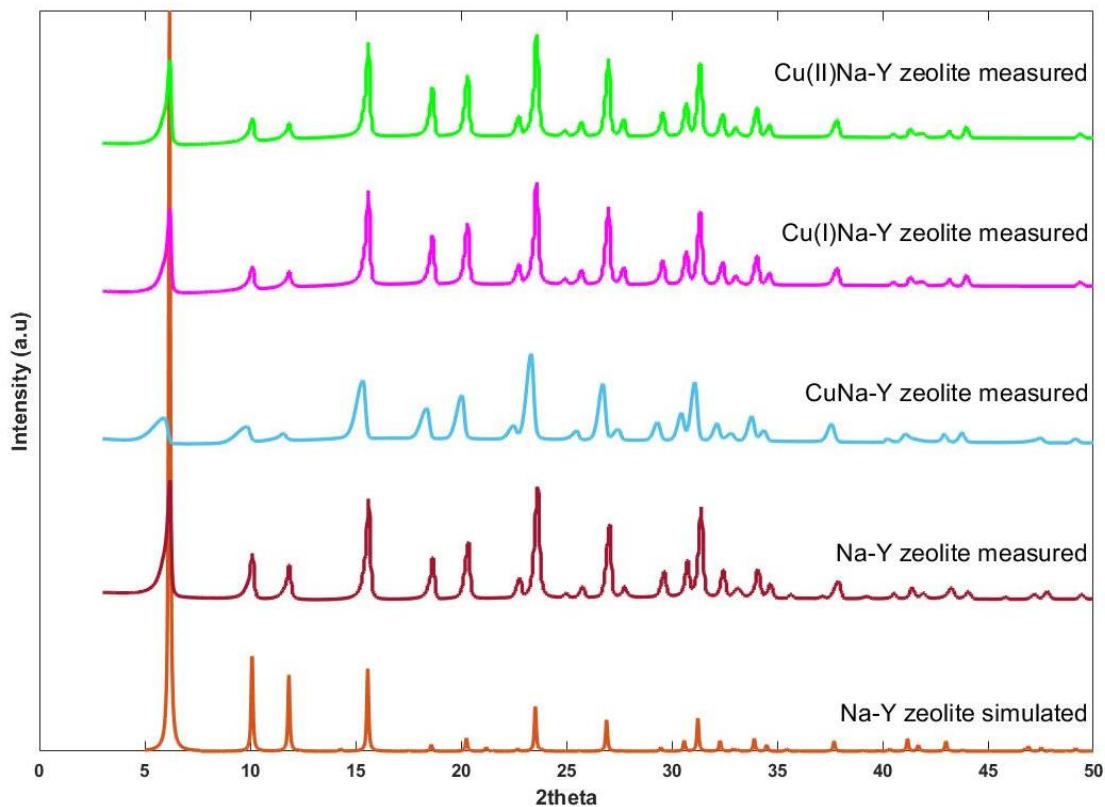


Figure 3.3.1-1. Measured XRD patterns of zeolitic materials. From top to bottom: Cu(II)Na-Y, Cu(I)Na-Y, CuNa-Y, Na-Y zeolites compared to the simulated XRD pattern of Na-Y zeolite. All XRD measurement were done under ambient conditions.

The H_2 -TPR experiments gave the results for the type of copper cation present in each tested zeolite. First, the results for Cu(I)Na-Y zeolite are presented.

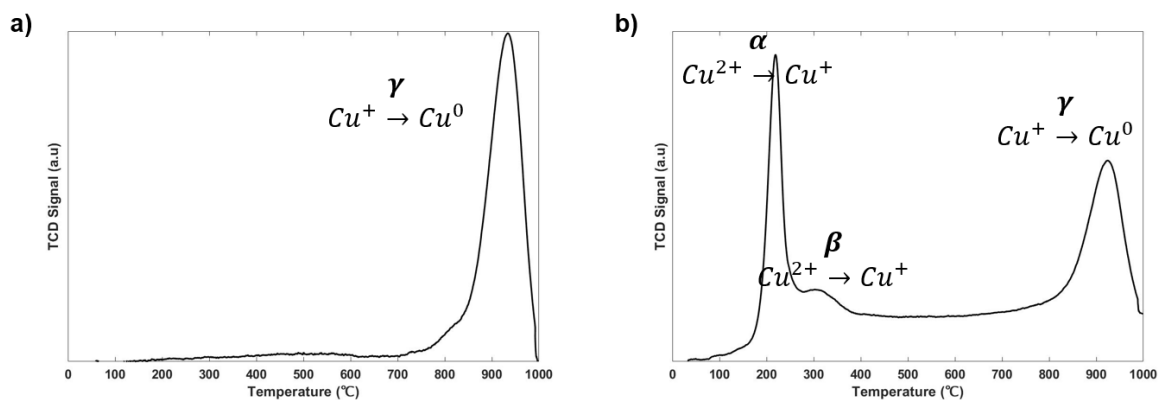


Figure 3.3.1-2. H_2 -TPR curves for Cu(I)Na-Y zeolite. a) H_2 -TPR analysis after in-situ activation of Cu(I)Na-Y zeolite. b) H_2 -TPR analysis after ex-situ activation of Cu(I)Na-Y zeolite.

The curves of the TCD signal versus temperature correspondent to Cu(I)-Na analyzed after in-situ and ex-situ reduction are shown in Figure 3.3.1-2. As seen in Figure 3.3.1-2 (a), there is only one peak appearing at temperature between 900°C and 1000°C. This result agrees what was reported by (Lobb, 2017), regarding the type of copper ion that is predominant in the copper zeolite after activation under hydrogen at 450°C. In that work, Cu(I)Na-Y zeolite was in-situ activated in the same Micromeritics Autochem and then it was analyzed by H_2 -TPR. Because in-situ activation avoided the sample to be exposed to air, the Cu(I) cations could be preserved in that oxidation state before the H_2 -TPR analysis started.

On the other hand, ex-situ activation of the zeolite, previous its H_2 -TPR analysis caused the zeolite to be exposed to air and that caused the oxidation of the Cu(I) cations back to Cu(II) cations. The H_2 -TPR result for this case is shown in Figure 3.3.1-2 (b), which shows the predominant copper cations in the zeolite were

Cu(II) cations. Because contact with air caused the oxidation of the Cu(I) cations back to Cu(II) cations, this may be the reason for both zeolites to show a similar desulfurization capacity in the following experiments.

Now, the H_2 -TPR results for Cu(II)Na-Y zeolite are shown. This zeolite was activated under dry air at 450°C, to favor the conversion of copper atoms to its Cu(II) oxidation state. As before, the copper zeolite was activated ex-situ and in-situ previous the H_2 -TPR analysis. The H_2 -TPR results for Cu(II)Na-Y are shown in Figure 3.3.1-3.

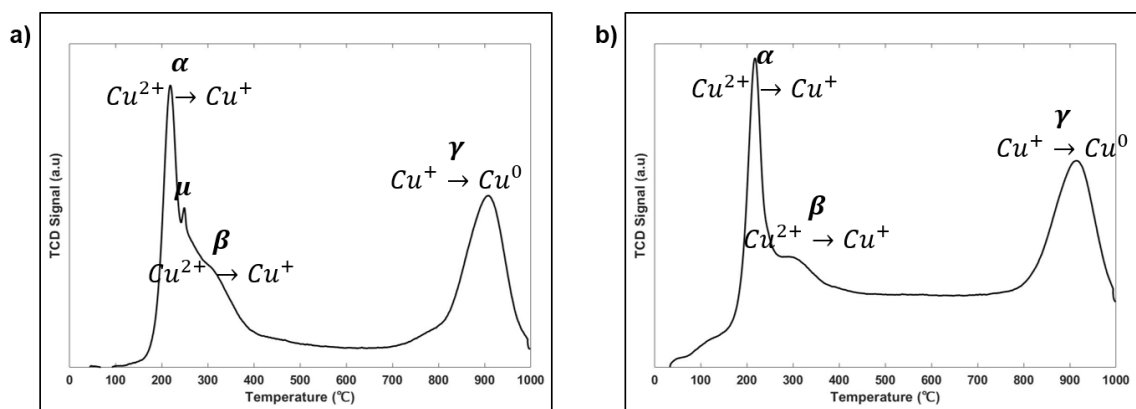


Figure 3.3.1-3. H_2 -TPR curves for Cu(II)Na-Y zeolite. a) H_2 -TPR analysis after in-situ activation of Cu(II)Na-Y zeolite. b) H_2 -TPR analysis after ex-situ activation of Cu(II)Na-Y zeolite.

For the sample activated in-situ in the Micromeritics Autochem, Figure 3.3.1-3 (a) shows the curve of TCD versus temperature of the TPR analysis done after in-situ activation of Cu(I)Na-Y zeolite. The curve shows four peaks which correspond to the different copper cations in the zeolite structure. The curve can be divided in low-temperature region and high-temperature region as reported in

(Lobb, 2017). In the low-temperature region, the peak at 210°C is named the α -peak and corresponds to the Cu(II) cations located in the super cage of the zeolite framework. A second peak, named peak β , which overlaps with peak α appears after 300°C and corresponds to the Cu(II) cations located in the sodalite cavities of the zeolite framework. A very little peak, peak μ , appears between peaks α y β . Peak μ corresponds to the copper atoms present as CuO which during the TPR analysis are reduced to metallic copper or Cu(0). These results agrees well with the work by (Lobb, 2017).

The H_2 -TPR analysis after ex-situ activation of Cu(II)Na-Y zeolite was also obtained. The curve of TCD versus temperature is shown in Figure 3.3.1-3 (b). The curve in Figure 3.3.1-3 (b) agrees well with the curve shown in Figure 3.3.1-3 (a); this indicates that Cu(II)Na-Y zeolite was less affected by its exposition to air, and that most copper atoms are present in the form of Cu(II) cations.

To estimate the amount of the copper species in each zeolite, the integration of the area under the TCD curves was done. The quantification was done based on the hydrogen consumption by each one of the species present in the zeolite while the samples were analyzed by H_2 -TPR. First, Table 3.3.1-1 shows the hydrogen consumption of each specie present in the zeolite samples.

Table 3.3.1-1. Hydrogen consumption during H_2 -TPR analysis of Cu(I)Na-Y and Cu(II)Na-Y zeolites

Sample	Peak α	Peak μ	Peak β	Peak γ
Cu(I)Na-Y In-situ	0 (0) ^a	0 (0)	0 (0)	13.0 (0.45)
Cu(I)Na-Y Ex-situ	9.5 (0.33)	-	3.2 (0.11)	13.1 (0.45)
Cu(II)Na-Y In-situ	11.4 (0.39)	0.11 (0.0)	6.5 (0.23)	12.3 (0.43)
Cu(II)Na-Y Ex-situ	12.5 (0.43)	-	5.3 (0.18)	12.1 (0.42)

^a The value outside the parenthesis indicates the volume of H_2 consumed per gram of activated adsorbent ($\frac{cm^3}{g}$). The value inside the parenthesis gives the number of moles of H_2 consumed per mole of Cu. The calculations were made assuming the ideal gas law with constant temperature of 100°C in the TCD. The hydrogen consumption error is $\pm 2\%$.

The percentages of each one of the copper species present in each zeolite were calculated following the work by Lobb (Lobb, 2017). The results are presented in Table 3.3.1-2.

Table 3.3.1-2. Quantification of copper species in Cu(I)Na-Y and Cu(II)Na-Y zeolites after in-situ and ex-situ activation. The results correspond to the percentage of each copper specie over the total copper mass in the respective zeolite sample.

Sample	Supercage Cu^{2+}	CuO and Cu^0	Sodalite Cavity Cu^{2+}	Cu^+
Cu(I)Na-Y In-situ	0%	10.1%	0%	89.9%
Cu(I)Na-Y Ex-situ	40.55%	12.54%	21.97%	24.94%
Cu(II)Na-Y In-situ	18.46%	30.17%	45.13%	6.24%
Cu(II)Na-Y Ex-situ	39.65%	23.42%	36.93%	0%

From Table 3.3.1-2, it can be seen that the content of Cu(I) cations decreased from 89.9% in the sample activated in-situ, to 24.94% in the sample activated ex-situ. The sample activated ex-situ was exposed to air while loading the Cu(I)Na-Y zeolite sample into the Autochem. That exposure to air was the cause for the Cu(I) cations to re-oxidize to Cu(II) cations. This results agrees well with the results presented in the work by Lobb (Lobb, 2017), who reported the fast re-oxidation of Cu(I) to Cu(II) when the samples Cu(I)Na-Y was exposed to air.

Comparing the percentage of Cu(II) cations in the Cu(I)Na-Y sample that was activated ex-situ with both Cu(II)Na-Y samples, Cu(I)Na-Y after being exposed to air had approximately the same amount of Cu(II) cations than Cu(II)Na-Y zeolite activated under the same conditions (ex-situ). This helps to explain why both materials showed almost the same sulfur capacity when used over model fuels and JP-8 in the following experiments.

3.3.2. Batch desulfurization of model fuels at elevated temperatures

Both Cu(I)Na-Y zeolite and Cu(II)Na-Y zeolite were used to desulfurize two model fuels, MF (n-dodecane, 3-MBT) and MFT (n-dodecane, 3-MBT, toluene) at 30°C, 80°C, 130°C, and 180°C. Figure 3.3.2-1 shows the sulfur capacity of each zeolite at the four temperatures when used on the MF samples.

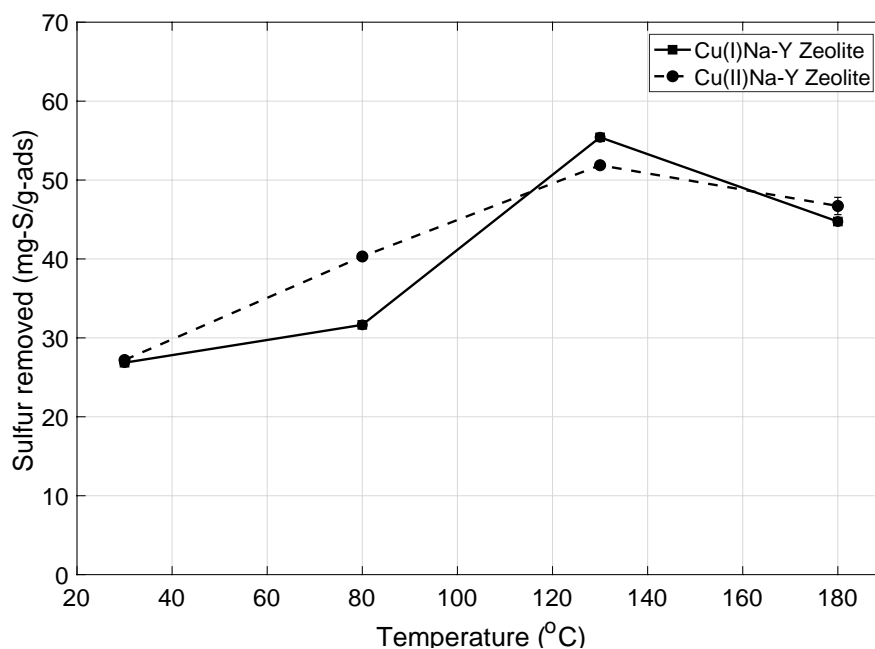


Figure 3.3.2-1. Total sulfur removed from MF versus temperature. Adsorbent materials were: squares-solid line for Cu(I)Na-Y, and dots-dashed line for Cu(II)Na-Y zeolite. The fuel used was MF (n-dodecane + 3MBT), 2000 ppmwS. Desulfurization time was 6 hours at 30°C, 80°C, 130°C, and 180°C.

Figure 3.3.2-1 shows that the sulfur capacity is almost the same at any temperature for both zeolites. This indicates that both Cu(I)Na-Y zeolite and Cu(II)Na-Y zeolite performed the same at any temperature when the fuel was formed only by n-dodecane and 3-MBT. The sulfur removal increased with temperature, having reached a maximum at 130°C, and then dropped at 180°C.

To study the effect of an aromatic compound on the sulfur removal by both Cu(I)Na-Y and Cu(II)Na-Y zeolites, the model fuel that contained toluene (MFT) was used in the desulfurization experiments. The results of those experiments are shown in Figure 3.3.2-2.

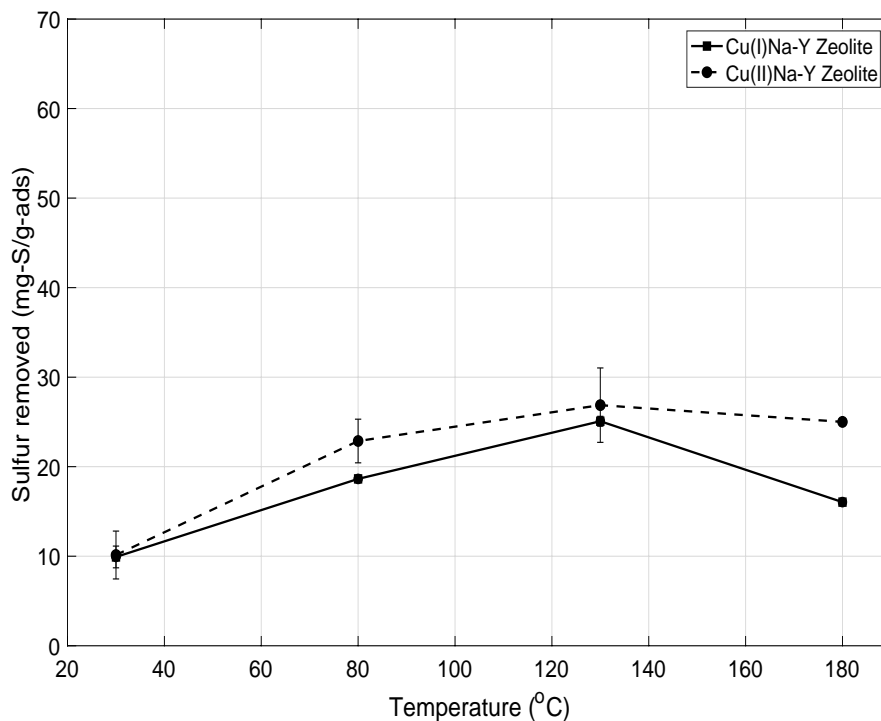


Figure 3.3.2-2. Total sulfur removed from MFT versus temperature. Adsorbent materials were: squares-solid line for Cu(I)Na-Y, and dots-dashed line for Cu(II)Na-Y zeolite. The fuel used was MFT (n-dodecane + 3MBT + 15%w toluene), 2000 ppmwS. Desulfurization time was 6 hours at 30°C, 80°C, 130°C, and 180°C.

Figure 3.3.2-2. shows the sulfur capacity of each zeolite at all four temperatures but now after the zeolites were used on the fuel samples MFT. MFT consisted of n-dodecane, 3-MBT, and toluene. Comparing Figure 3.3.2-1 with Figure 3.3.2-2, the desulfurization trend is the same for both model fuels; the sulfur capacity tends to increase with temperature, reaching a maximum at 130°C, and decreasing at 180°C.

Figure 3.3.2-2 shows a clear decrease in the overall sulfur capacity of both zeolites at all temperatures if compared to the results presented in Figure 3.3.2-1. This was a consequence of the presence of an aromatic compound in the tested fuel (MFT). Aromatic molecules can compete for the metal sites available in the adsorbents and as a result a lower sulfur removal was achieved. Although the sulfur removal decreased because of the toluene molecules, the overall sulfur removal followed the same trend; it increased as the work temperature increased reaching a maximum value at 130°C.

3.3.3. Batch desulfurization of JP8 at elevated temperatures

Cu(I)Na-Y and Cu(II)Na-Y zeolites were also used in batch desulfurization experiments using a real jet fuel: JP8. As before, the experiment conditions were 6 hours of contact time between the fuel and the adsorbent, and four work

temperatures, 30°C, 80°C, 130°C, and 180°C. The mass of adsorbent used was 200 mg and the volume of fuel used was 20 mL.

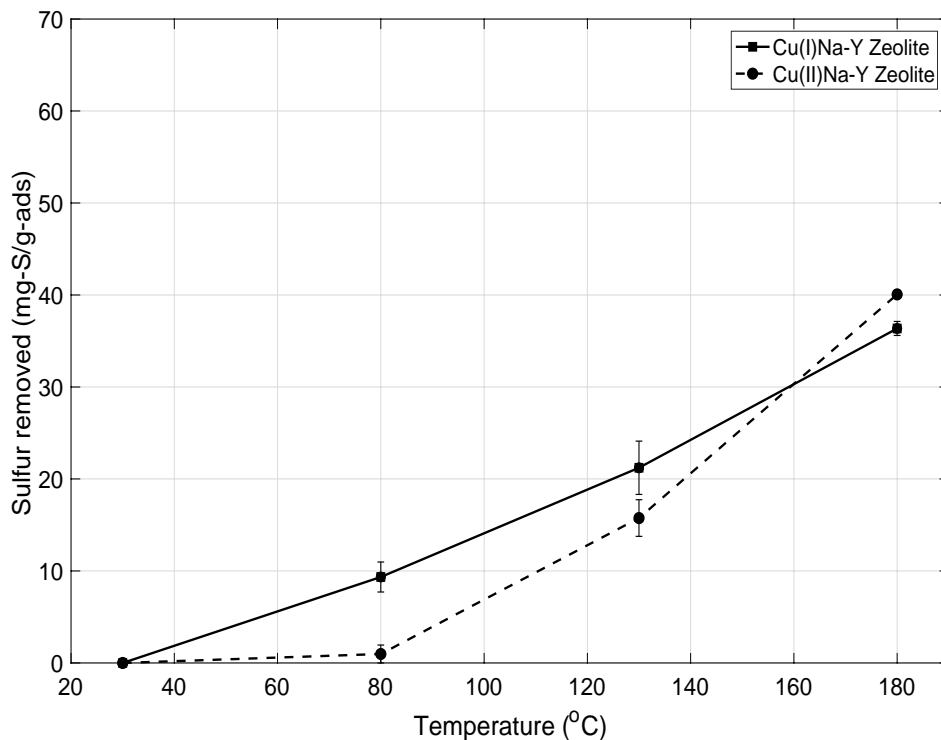


Figure 3.3.3-1. Total sulfur removed from JP-8 versus temperature. Adsorbent materials were: squares-solid line for Cu(I)Na-Y, and dots-dashed line for Cu(II)Na-Y zeolite. The fuel used was JP-8, 2230 ppmwS. Desulfurization time was 6 hours at 30°C, 80°C, 130°C, and 180°C.

As Figure 3.3.3-1 shows, both Cu(I)Na-Y and Cu(II)Na-Y zeolites followed the same desulfurization trend when used with JP-8. The sulfur removal was near zero at the lowest temperature (30°C) and increased as the work temperature increased. The maximum sulfur removal was achieved at 180°C. The results shown in Figure 3.3.3-1 indicate that both zeolites achieved almost the same sulfur capacity when the work temperature increased. This may be an indication that the copper

cations in both zeolites followed the same adsorption mechanism at elevated desulfurization temperatures.

3.3.4. GC-PFPD test of treated JP-8 samples

The efficacy of both Cu(I)Na-Y and Cu(II)Na-Y adsorbents was tested by using them in batch desulfurization of real JP-8. After that, the treated fuel samples were tested by GC-PFPD using the program described in Table 2.2.6-1. As shown in Figure 3.3.3-1, the highest sulfur removal was achieved when the work temperature was 180°C, and both zeolites reached approximately the same sulfur removal.

Figure 3.3.4-1 shows the chromatograms for the JP-8 samples treated with Cu(I)Na-Y zeolite.

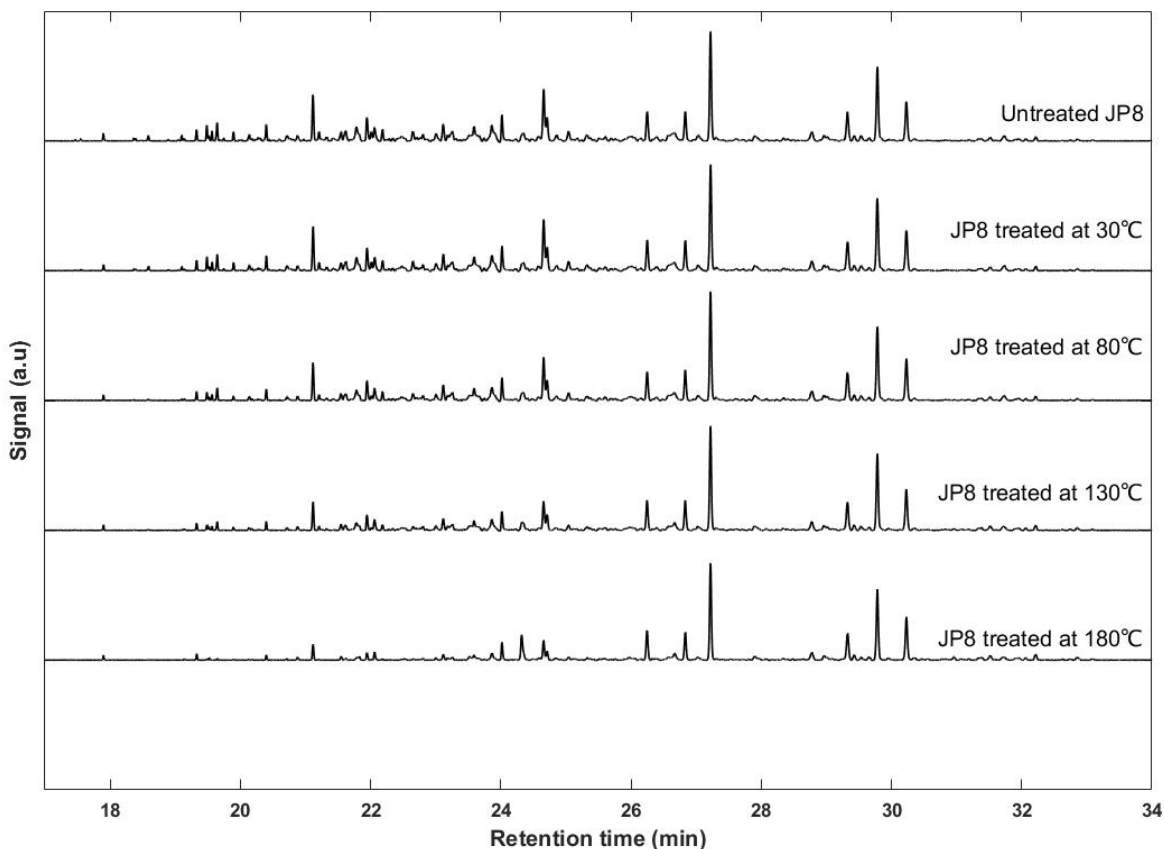


Figure 3.3.4-1. GC-PFPD results for JP-8 treated with Cu(I)Na-Y zeolite. From top to bottom: Untreated JP-8, JP-8 treated at 30°C, 80°C, 130°C, and 180°C.

As Figure 3.3.4-1 shows, the chromatograms of the JP-8 samples after they were treated with Cu(I)Na-Y zeolite at the different temperatures kept the same sulfur matrix of untreated JP-8. There were no new compounds formed after the treatment. The main difference was the decrease in the relative area of the peaks correspondent to those compounds that eluted between 17 and 25 min. As happened with the regular CuNa-Y zeolite, the lighter sulfur compounds were removed first when the fuel was treated with Cu(I)Na-Y zeolite and elevated temperatures. The greatest sulfur removal was achieved at 180°C.

The chromatograms for the JP-8 samples treated with Cu(II)Na-Y zeolite are presented in Figure 3.3.4-2.

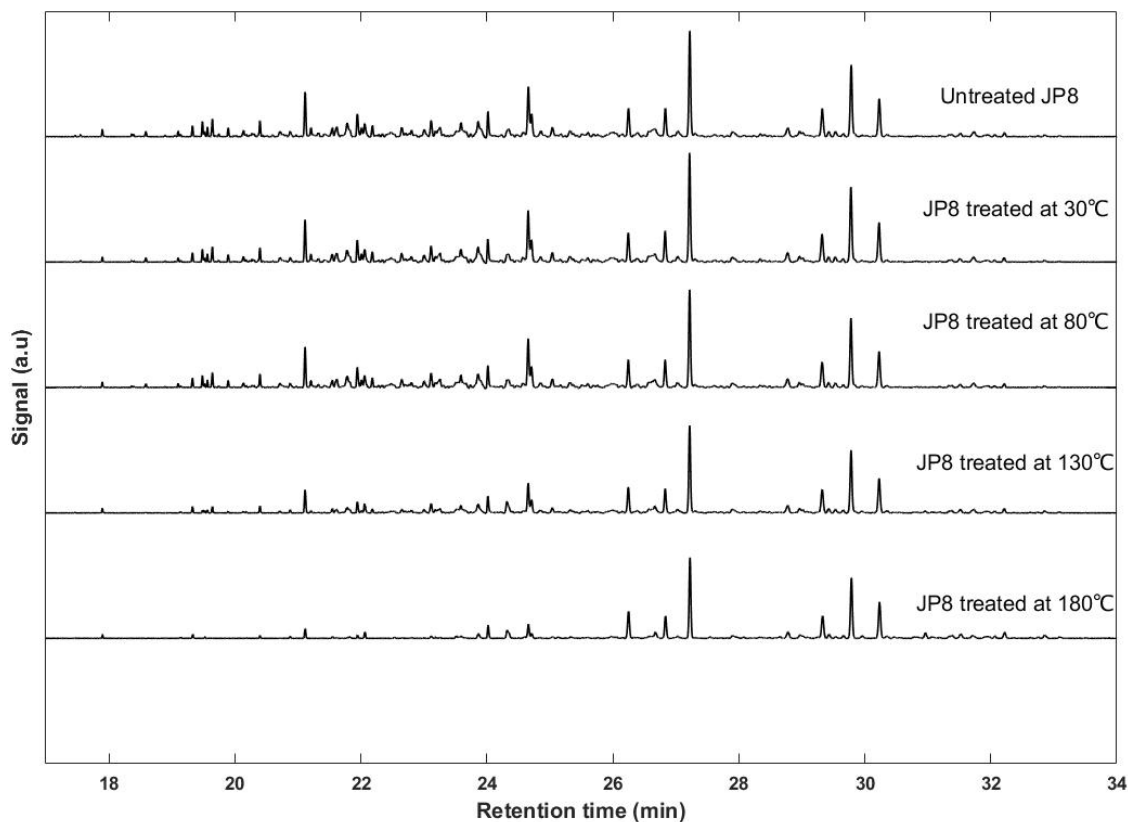


Figure 3.3.4-2. GC-PFPD results for JP-8 treated with Cu(II)Na-Y zeolite. From top to bottom: Untreated JP-8, JP-8 treated at 30°C, 80°C, 130°C, and 180°C.

The results shown in Figure 3.3.4-1 are very similar to those of Figure 3.3.4-2. Again, the sulfur matrix of JP-8 was kept after the desulfurization treatment. There were no new compounds formed by the treatment with Cu(II)Na-Y zeolite, and the most notorious difference observed in Figure 3.3.4-2 is the decrease of the relative area of the peaks between 17 and 25 min. Those peaks correspond to the lighter or lower-boiling point sulfur compounds in the fuel which were removed first by the desulfurization treatment with Cu(II)Na-Y zeolite.

3.4. Conclusions

The desulfurization experiments done on model fuels (MF and MFT), and real jet fuel (JP-8) showed similar results when the adsorbent was Cu(I)Na-Y or Cu(II)Na-Y zeolite. As first it was thought that both zeolites performed the same at elevated temperatures, no matter the type of copper cation was present in their structure. But the H_2 -TPR results gave evidence of the fast reoxidation of the Cu(I) cations. When Cu(I)Na-Y was handled and placed into the fuel to start the batch desulfurization experiments, it could have been in contact with air and some of its Cu(I) cations oxidized back to Cu(II). All the experiments that involved Cu(I)Na-Y zeolite were prepared in a glove-bag filled with UHP-Argon gas, but there was no device to measure the oxygen content in the system. Also, the oxygen content in JP-8 should be considered. The fuel samples were not degassed before performing the experiments, and any diluted oxygen in the fuel could have also caused the oxidation of the Cu(I) cations in Cu(I)Na-Y zeolite. As a result, Cu(I)Na-Y zeolite became similar to Cu(II)Na-Y and CuNa-Y zeolites which have a portion of Cu(II) in their structures.

Adsorptive desulfurization of JP-8 using UiO-66 metal-organic frameworks (MOFs)

4.1. Introduction

Among the different adsorbents tested for adsorptive desulfurization, metal-organic frameworks (MOFs) have shown good performance to remove sulfur compounds from model fuel due to their great surface area and porosity. However, the effectiveness of MOFs to remove sulfur from real jet fuel has not been studied deeply. This chapter focuses on the use of the UiO-66 metal-organic framework as adsorbent in adsorptive desulfurization of JP-8 at elevated temperatures. In addition, two other materials were prepared, UiO-66-10 and UiO-66-25, which are defective versions of the pristine UiO-66 MOF. These two adsorbents were prepared varying the content of hydrochloric acid (HCl, 37% purity) in the preparation of

UiO-66. Modifying the content of HCl during the preparation of the MOF creates defects in its structure (Clark, Heck, Powell, & Wong, 2019) that can be useful for sulfur removal by providing bigger pores that can accommodate better the bigger sulfur molecules present in JP-8 such as 2,3,7-trimethylbenzothiophene.

UiO-66-10 corresponds to the material prepared with 10% of HCl, while UiO-66-25 corresponds to a HCl content of 25% (Clark et al., 2019). The pristine UiO-66 is referred as UiO-66-DF because the process used for its preparation has been reported as to produce a MOF with very little amount of defects in its structure (Shearer et al., 2014).

4.2. Experimental work

4.2.1. Synthesis of UiO-66 metal-organic framework adsorbents

Defective UiO-66 metal-organic framework adsorbents were synthesized to test if adsorbents with bigger pore sizes and greater surface areas may perform well in adsorptive desulfurization of JP-8. Two defective UiO-66 adsorbents (UiO-66-10 and UiO-66-25) were prepared using hydrochloric acid as modulator. UiO-66 refers to the parent metal-organic framework (UiO-66), and the number after it (10 or 25) refers to the percentage of hydrochloric acid used in their synthesis. Defect free UiO-66 was also synthesized and used for comparison; this material will be referred as UiO-66-DF, where DF stands for Defect-Free.

For synthesizing all three adsorbents, the following materials were used: $ZrCl_4$ ($\geq 99.5\%$ metal basis, powder), terephthalic acid (98% powder), and N,N-dimethylformamide ($\geq 99.9\%$, liquid) were purchased from Sigma Aldrich. Methanol ($\geq 99.9\%$, liquid) was purchased from Fisher Scientific. Hydrochloric acid (36.5 – 38%) was purchased from EMD Millipore.

The procedures for the synthesis of all three adsorbents are described as follows.

4.2.1.1. Synthesis of UiO-66-10 and UiO-66-25 adsorbents

For the synthesis of **UiO-66-10** and **UiO-66-25** adsorbents, the procedure from (Clark et al., 2019) was followed. 3.2 mmol of $ZrCl_4$ were added to a 250 mL flask, then 10 mL (for UiO-66-10) or 25 mL (for UiO-66-25) of hydrochloric acid (HCl) were added. The solution volume was adjusted to 50 mL with N,N-dimethylformamide (DMF). The solution was sonicated until all solids dissolved. After that, 3.2 mmol of terephthalic acid were added to the solution, and then the solution was adjusted to 100 mL with DMF. The new solution was sonicated for 30 min and then it was equally divided into four 40 mL glass vials. The sealed vials were put in a preheated oven at 120°C for 24 hours. After heating, the formed precipitate of each vial was recovered by vacuum filtration. The precipitate was washed three times with 10 mL of DMF and three times with 10 mL of methanol. The vacuum filtration continued until no solvent was present and the solid precipitate removed easily from the filter paper. For activating the adsorbent, the

precipitate was let to dry overnight in a vacuum oven at 150°C to remove the trapped solvent and create the porous structure. The activated material was stored in a desiccator ready to be used. A schematic for the synthesis procedure of defective UiO-66 adsorbents is shown in Figure 4.2.1-1.

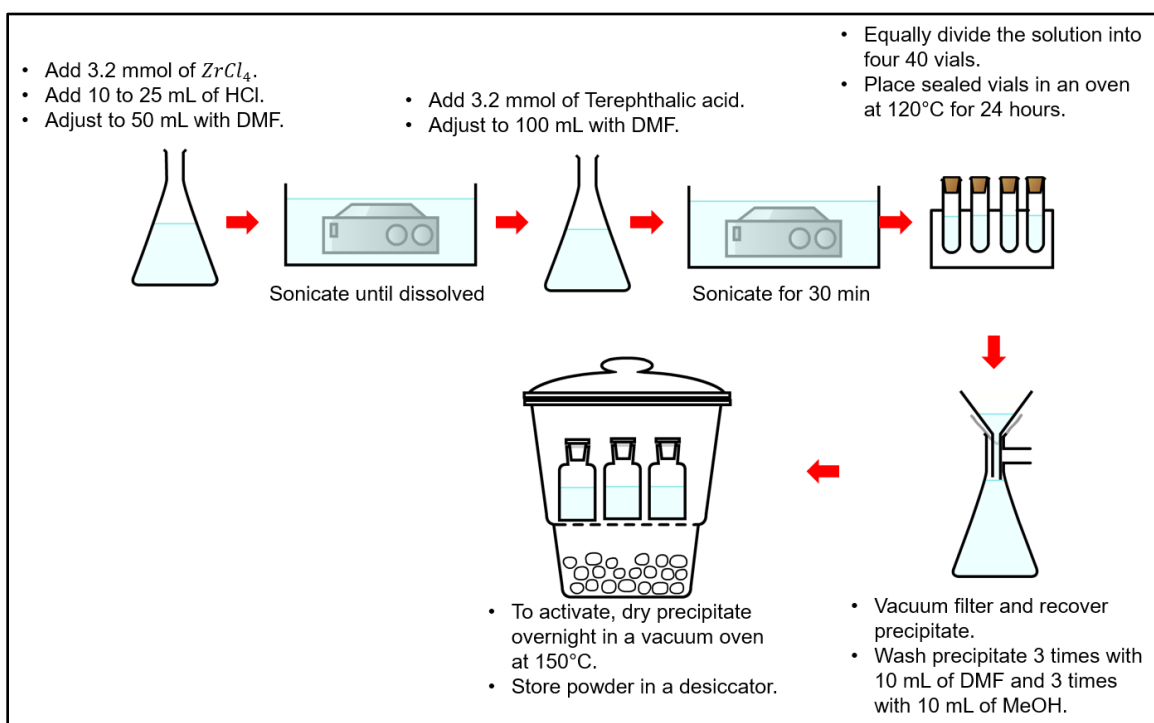


Figure 4.2.1-1. Procedure for the synthesis of defective UiO-66 adsorbents (UiO-66-10 and UiO-66-25)

4.2.1.2. Synthesis of UiO-66-DF adsorbent

For the synthesis of the **UiO-66-DF** adsorbent, the procedure from (Shearer et al., 2014) was followed. 97.4 mL of DMF were added to a 250 mL flask with 16.2 mmol of $ZrCl_4$ and 2.86 mL of HCl. The solution was sonicated until all solids

dissolved or up to 30 min maximum. Then, 5.39 g of terephthalic acid were added to the solution and it was sonicated again for 30 min. The solution was equally divided in four aliquots and each aliquot was transferred to a 100 mL PTFE liner. Each liner was sealed and placed in a stainless-steel autoclave. The autoclaves were placed in a pre-heated oven at 220°C for 20 hours. After heating, the formed precipitate of each liner was recovered by vacuum filtration. Each precipitate was washed three times with DMF and three times with methanol and then, it was vacuum filtered until no solvent remained. For activating the adsorbent, the material was dried overnight in a vacuum oven at 150°C. After activation, the adsorbent was stored in a desiccator. Figure 4.2.1-2 shows a schematic of the synthesis of UiO-66-DF.

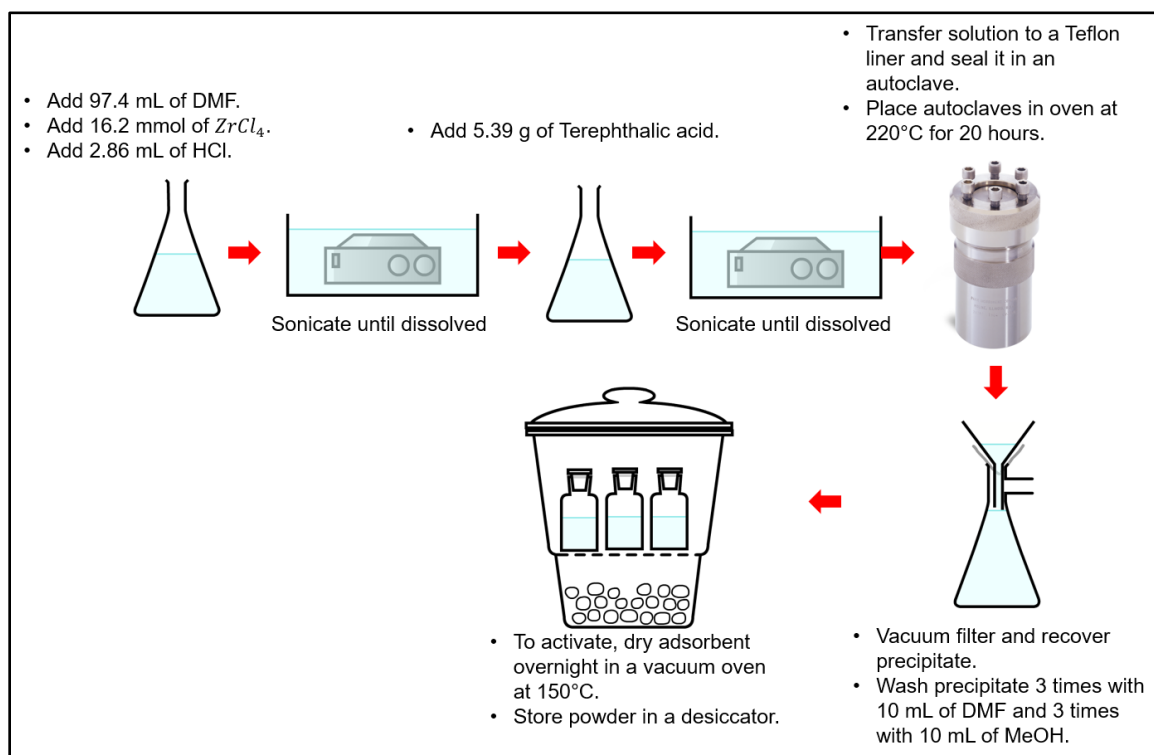


Figure 4.2.1-2. Procedure for the synthesis of defect-free UiO-66 adsorbent (UiO-66-DF)

4.2.2. Characterization of UiO-66 metal-organic framework adsorbents

Powder X-ray diffraction (XRD) measurements of the defective UiO-66 adsorbents (UiO-66-10 and UiO-66-25) were performed to confirm that they had the same crystalline structure as the pristine or defect-free UiO-66 metal organic framework. The measurements were performed in a Rigaku D/Max (EAST) Ultima II diffractometer, using Cu-K α radiation. The 2θ measurement range was 3 - 50°. The measured patterns were then compared to the simulated pattern of UiO-66 metal organic framework. As before, the simulated pattern was obtained using the software Mercury 3.10.3 provided by The Cambridge Crystallographic Data Centre (CCDC).

Since the procedure for the synthesis of UiO-66-10 and UiO-66-25 adsorbents was taken from the work by Clark and coworkers (Clark et al., 2019), the values of surface area and pore diameter for each UiO-66 adsorbent are also reported from that work. Clark and coworkers reported that the surface areas were calculated using the Brunauer-Emmett-Teller (BET) model. For the calculation of the pore size distributions, Clark and coworkers used the nonlocal density functional theory (NL-DFT) for which it was assumed the pores followed cylindrical pore geometry.

4.2.3. Batch desulfurization of JP-8 at elevated temperatures

As explained in section 2.2.4, the desulfurization experiments were done in polyethylene liners and stainless-steel vessels. 20 mL of jet fuel were transferred to the liner and then 200 mg of the adsorbent were added. The liner was covered with its cap and located into a stainless-steel vessel. Next, the vessel was closed tightly and secured with 8 bolts. Each vessel was located into an oven set at the desired temperature, 30°C, 80°C, 130°C, or 180°C, for 6 hours.

After 6 hours, the oven temperature was set to 25°C and the adsorbent material was recovered through vacuum filtration. The treated fuel was stored in a glass vial. The wet adsorbent was put to dry on a petri dish for 24 hours. Then, the dry adsorbent was collected into a glass vial.

4.2.4. Total sulfur content measurement

Each jet fuel sample was tested by X-ray Fluorescence (XRF) to measure its total sulfur content. The measurements were done in an XRF sulfur analyzer, Sindie 7039 manufactured by X-Ray Optical Systems (XOS).

4.2.5. GC-PFPD test of treated JP-8 samples

Gas Chromatography was used to analyzing the treated jet fuel samples to investigate for any change in their sulfur matrix. The system consisted of a gas chromatographer, Agilent 6890N series, coupled to a Pulsed Flame Photometric Detector (PDPF), model 5380 by OI Analytical, which is specific to sulfur. A complete

description of the gas chromatography system configuration is presented in Table 2.2.6-1.

4.3. Description of results and analysis

4.3.1. Characterization of UiO-66 adsorbents: XRD patterns and surface properties

The measured XRD patterns for UiO-66-10, UiO-66-25, and UiO-66-DF are presented in Figure 4.3.1-1. The simulated XRD pattern for UiO-66 is also shown for comparison. The simulated pattern of UiO-66 shown in Figure 4.3.1-1 corresponds to the **fcu**-topology.

All the measured XRD patterns corresponded well with the simulated pattern of **fcu** UiO-66 which indicates that for the adsorbents formulated with 10% and 25% of HCl, the crystalline structure of the metal-organic framework was successfully achieved after synthesis.

The XRD pattern for UiO-66-DF showed a pattern that also agreed with the simulated one, indicating that the expected **fcu**-topology was also achieved for that adsorbent. The **fcu**-topology of UiO-66 metal-organic framework is depicted in Figure 4.3.1-2.

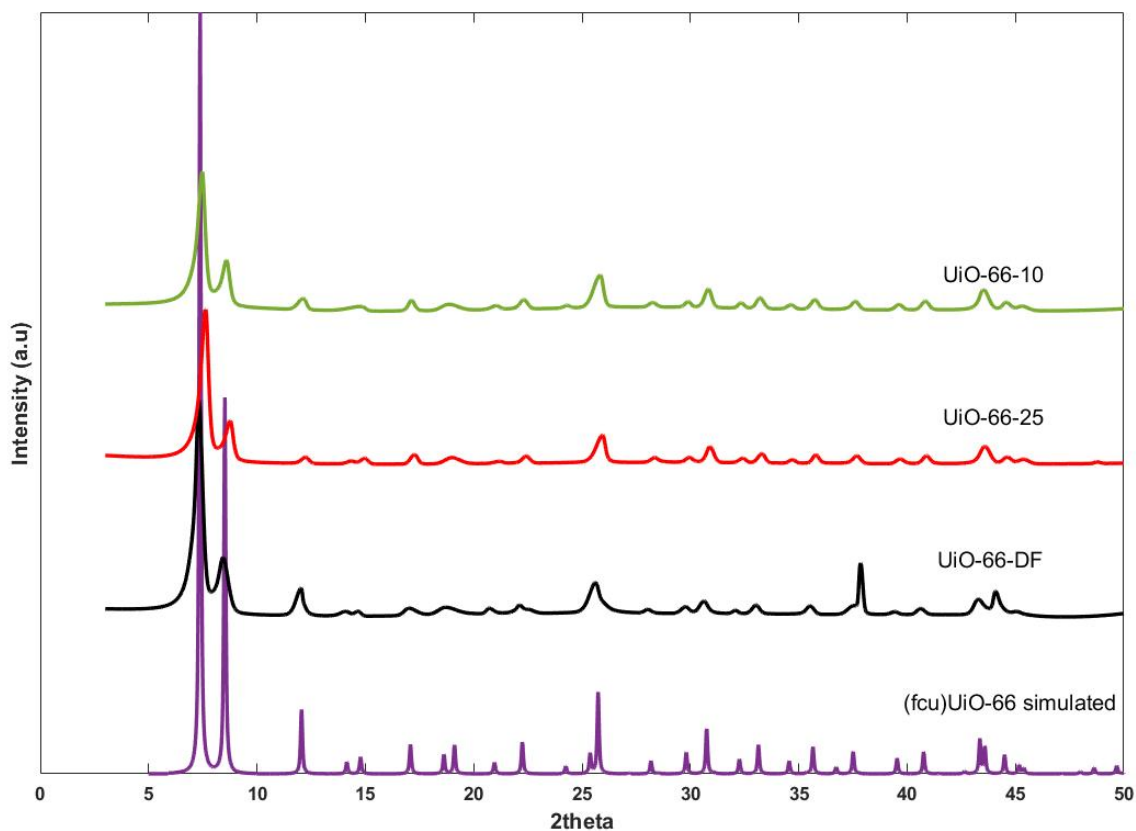


Figure 4.3.1-1. Measured XRD patterns of UiO-66 metal-organic framework adsorbents. The simulated XRD pattern of pristine UiO-66 is also shown for comparison.

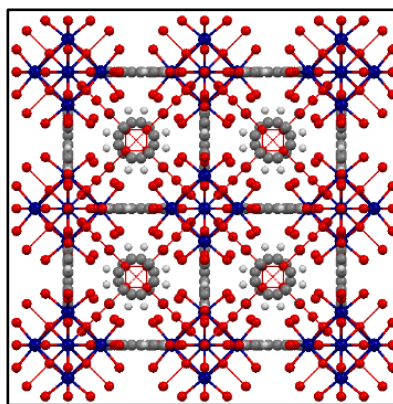


Figure 4.3.1-2. [001] view of fcu UiO-66 metal-organic framework. Atoms are colored as follows: O, red; Zr, blue; C, grey; H, white. Model was produced using the software Mercury 3.10.3 provided by The Cambridge Crystallographic Data Centre (CCDC).

The reported values of surface area and pore diameters for the UiO-66 adsorbents are listed in Table 4.3.1-1. These results were taken from (Clark et al., 2019). Table 4.3.1-1 also shows the reported values for Na-Y and ion-exchange CuNa-Y zeolites.

Table 4.3.1-1. Surface properties of synthesized UiO-66 adsorbents (Clark et al., 2019)

Adsorbent	BET surface area $\left(\frac{m^2}{g}\right)$	Pore diameter (nm)
UiO-66-10	1423	0.8 – 2.0
UiO-66-25	1404	0.8 – 2.0
UiO-66-DF	1121	0.8 – 1.1
Na-Y zeolite*	650	0.8 – 1.2
CuNa-Y zeolite*	623	0.8 – 1.2

*Data taken from Table 2.3.1-1.

As Table 4.3.1-1 shows, the UiO-66 metal-organic framework materials had two times the surface area of the zeolitic materials. Regarding their pore size, the pristine or defect-free UiO-66 had a pore size similar to that of the zeolitic materials.

The adsorbents UiO-66-10 and UiO-66-25 that were synthesized to create defects in their structures, had bigger pores with diameters between 0.8 and 2.0 nm which are greater than the pores of NaY and CuNa-Y zeolites.

4.3.2. Batch desulfurization of JP-8 at elevated temperatures

The UiO-66 metal-organic framework materials were used in batch desulfurization experiments of real JP-8 at different temperatures; 30°C, 80°C, 130°C, and 180°C. The total sulfur removed results for each adsorbent and for each temperature are shown in Figure 4.3.2-1.

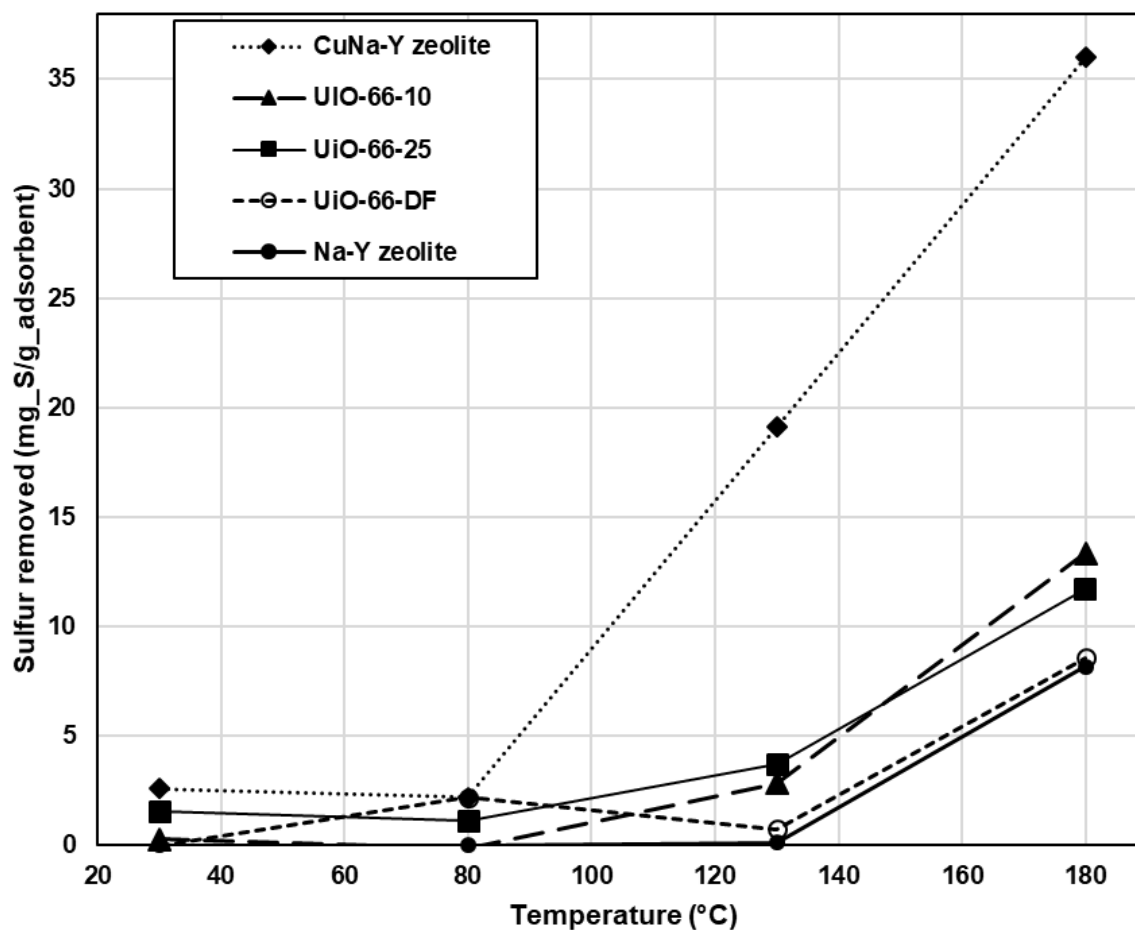


Figure 4.3.2-1. Total sulfur removed from JP-8 versus temperature. Adsorbent materials were: diamond-dots line for CuNa-Y zeolite, triangles-dash line for UiO-66-10, squares-solid line for UiO-66-25, circles-dash line for UiO-66-DF, and solid dots-solid line for Na-Y zeolite. The fuel used was JP-8, 2230 ppmwS. Desulfurization time was 6 hours at 30°C, 80°C, 130°C, and 180°C.

As shown in Figure 4.3.2-1, the three UiO-66 adsorbents performed similarly being UiO-66-10 the one that reached the higher sulfur removal of them. However, CuNa-Y zeolite was still the adsorbent that achieved the best sulfur removal in this study, reaching a sulfur capacity of 36 mg_S/g_adsorbent at 180°C. As observed for the zeolitic adsorbents, the same adsorption trend was observed for the UiO-66

adsorbents; the sulfur removal increases as the working temperature increases, which indicates that temperature has a positive effect on the adsorption process by increasing the diffusion of the sulfur compounds throughout the adsorbent or by allowing the formation of a more specific bond between the metal sites in the adsorbents and the sulfur compounds.

4.3.3. GC-PFPD test of treated JP-8 samples

The JP-8 samples treated with the UiO-66 adsorbents were analyzed by GC-PFPD to determine if any new sulfur compound was formed by the treatment. The chromatograms for each adsorbent at the four different temperatures are shown as follows. Figure 4.3.3-1 presents the chromatograms of the JP-8 samples treated with UiO-66-10 metal-organic framework. As can be seen, no new sulfur compounds were detected after the fresh JP-8 was treated using UiO-66-10 at the four work temperatures. Also, although the sulfur removal when using the UiO-66-10 adsorbent and elevated temperatures was lower than that reached with CuNa-Y zeolite, a common behavior was observed for both materials. The UiO-66-10 metal-organic framework started removing the smaller or lower boiling points sulfur compounds as well as what was observed for the CuNa-Y zeolite.

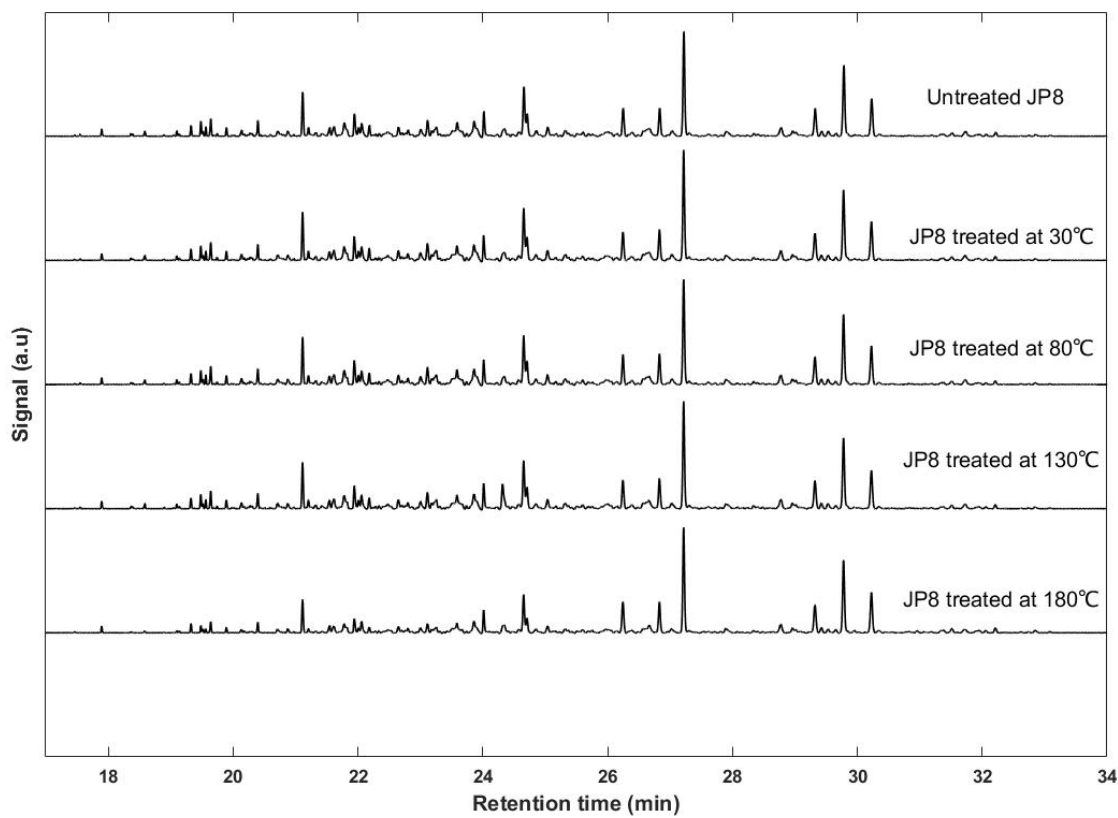


Figure 4.3.3-1. GC-PFPD signal for JP-8 treated with UiO-66-10 metal-organic framework. From top to bottom: Untreated JP-8, JP-8 treated at 30°C, 80°C, 130°C, and 180°C.

For the samples treated with UiO-66-25 and UiO-66-DF, their chromatograms are shown in Figure 4.3.3-2 and Figure 4.3.3-3 respectively. The sulfur removal reached by these last adsorbents was lower than that reached by UiO-66-10 and CuNa-Y zeolite. As before, no new sulfur compounds were detected in the chromatograms.

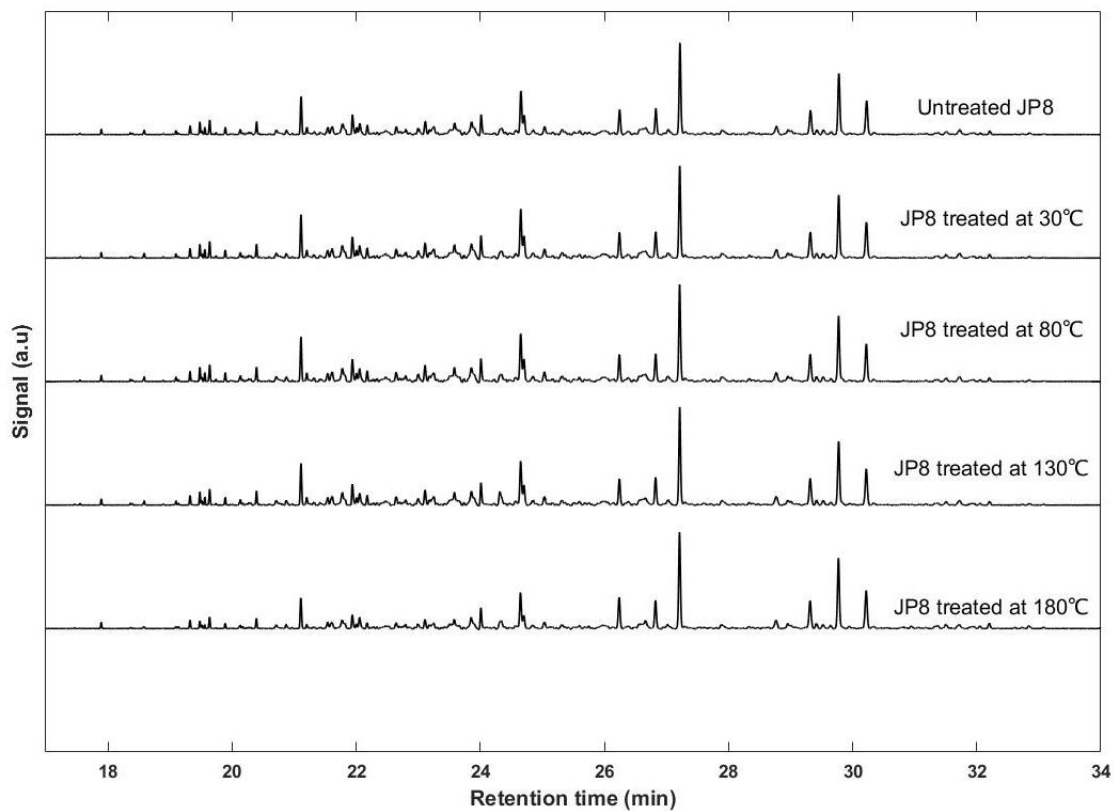


Figure 4.3.3-2. GC-PFPD signal for JP-8 treated with UiO-66-25 metal-organic framework. From top to bottom: Untreated JP-8, JP-8 treated at 30°C, 80°C, 130°C, and 180°C.

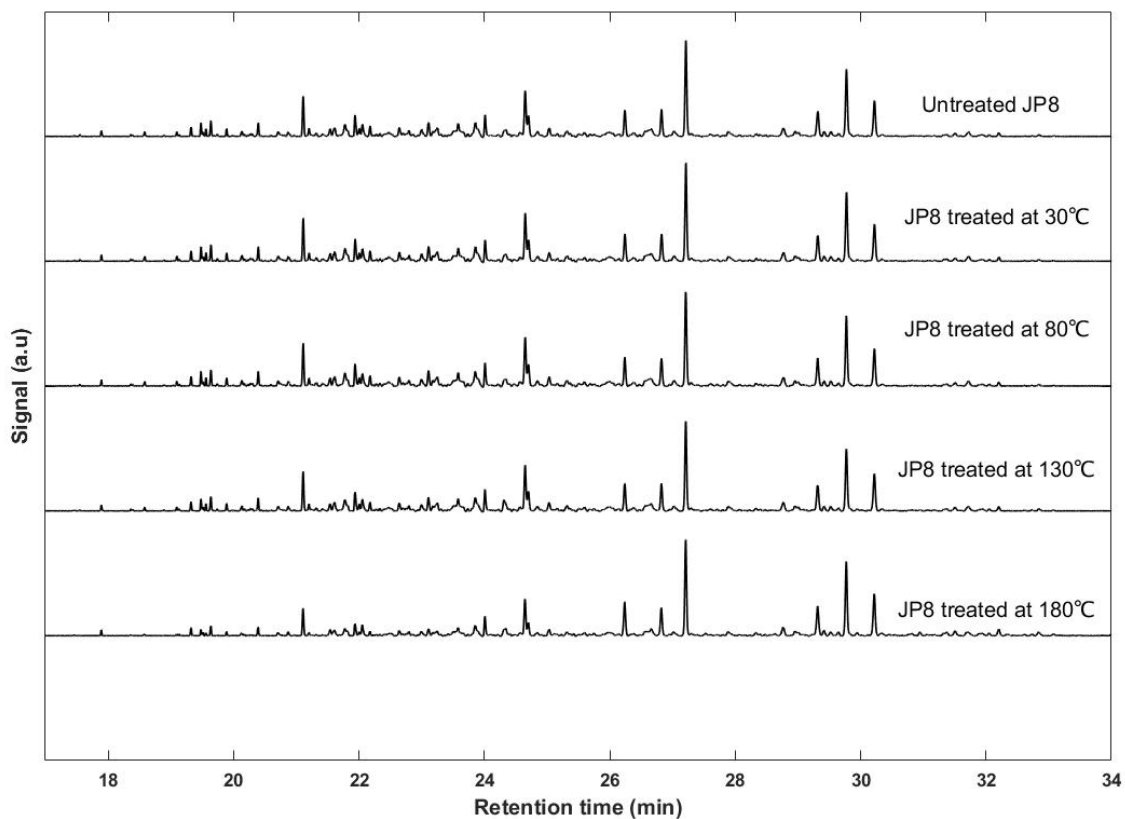


Figure 4.3.3-3. GC-PFPD signal for JP-8 treated with UiO-66-DF metal-organic framework. From top to bottom: Untreated JP-8, JP-8 treated at 30°C, 80°C, 130°C, and 180°C.

4.4. Conclusions

The inclusion of defects in the structure of the UiO-66 metal-organic framework created the availability of metal sites (Zr atoms) that may have adsorbed sulfur compounds. The inclusion of defects also allowed the creation of slightly bigger pores which could have helped to a better diffusion of the sulfur compounds. These effects were only reflected in the better sulfur removal achieved by the UiO-

66-10 adsorbent compared to the results for the pristine UiO-66-DF and the UiO-66-25 adsorbent which showed a lower sulfur capacity.

Compared to the performance of the zeolitic materials, the sulfur capacity of the UiO-66 adsorbents was much lower than the sulfur capacity of the CuNa-Y zeolite. This happened because the UiO-66 adsorbents did not have copper cations on their structures. Although, there were some zirconium atoms exposed in the defective UiO-66 adsorbents, those Zr atoms did not connect that strongly to the sulfur molecules as the copper cations in CuNa-Y zeolite.

Among the UiO-66 adsorbents, UiO-66-10 reached the highest sulfur removal from JP-8 at 180°C, which was still lower than the sulfur removal achieved by CuNa-Y zeolite.

Chapter 5

Future work

The main contribution of this thesis has been understanding how the sulfur compounds from JP-8 are removed by CuNa-Y zeolite at elevated temperatures. For this, Gas Chromatography coupled to Pulsed Flame Photometric Detector (GC-PFPD) was used to monitoring the JP-8 fuel samples after their treatment with all the adsorbent materials tested in this work. The main result was the observation that the lighter or low boiling points sulfur compounds were removed preferentially in the adsorptive desulfurization process by CuNa-Y zeolite when the process occurred at the highest temperature, 180°C. But, as it was shown by the desulfurization by steps experiments using CuNa-Y zeolite 180°C, after the removal of the lower boiling points sulfur compounds from JP-8, the removal of the higher boiling points sulfur compounds was also possible. This demonstrated that CuNa-Y zeolite can remove all sulfur compounds from JP-8 no matter their size. All these results contributed to the

completion of the manuscript by Priscilla Dias da Silva and coworkers which has already been submitted (Dias da Silva et al., 2019).

Certainly, the elevated temperature has a positive effect on the adsorptive desulfurization process by promoting the adsorption of sulfur compounds by CuNa-Y zeolite. This could be related to the creation of a stronger bond between the copper ions in the zeolite and the sulfur compounds of the fuel, as has been reported by (Dias da Silva et al., 2019).

As mentioned before, gas chromatography coupled to pulsed flame photometric detector (GC-PFPD) was useful to monitoring the JP-8 fuel samples after their treatment. Using this technique, it was possible to conclude that no new sulfur compounds were formed by the desulfurization process, however it was not possible to identify each sulfur compound present in the JP-8 sulfur matrix due to its complexity. The identification and quantification of each sulfur compound in JP-8 is another research interest that requires more work.

Regarding the production of the Cu(I)Na-Y and Cu(II)Na-Y zeolites, their H_2 -TPR results confirmed the fast reoxidation of the reduced Cu(I) cations back to Cu(II) cations which agrees well with the findings in the work by Lobb (Lobb, 2017). This was the reason for the zeolites to achieve a similar sulfur capacity at all four temperatures. More work needs to be done in this area to develop a method for reducing the CuNa-Y zeolite and make sure that the sample keeps protected from air during the preparation of the desulfurization experiments. Also, the oxygen content

of the fuel must be considered for future experiments, since that may be another source for the reoxidation of the Cu(I) cations.

The desulfurization results for the UiO-66 adsorbents showed that the material synthesized with 10% of HCl as modulator (UiO-66-10) reached the highest sulfur capacity of the three UiO-66 materials tested. However, the sulfur removal was still lower than that reached by CuNa-Y zeolite. The increased sulfur capacity of UiO-66-10 compared to the non-defective adsorbent (UiO-66-DF) indicated that the inclusion of defects may have helped to improve the adsorptive performance of the material. Thanks to the tunability of metal-organic frameworks, other strategies as functionalization of the UiO-66 metal-organic framework may result in a material more selective to sulfur compounds that can reach a higher sulfur removal.

Since the copper atoms in CuNa-Y zeolite are in part responsible for the its high sulfur capacity, the addition of copper cations to the structure of the UiO-66 metal-organic framework may be a good strategy to produce an effective adsorbent for adsorptive desulfurization of JP-8. The work by Hu and coworkers reported the synthesis of a UiO-66 material with detectable mesopores (3.9 nm) and the highest BET surface area of all UiO-66 materials so far with a value of $1730 \frac{m^2}{g}$. After successfully synthesizing this material, they determined the optimal conditions for ligand-exchange reactions which allowed them to perform the metalated-ligand-exchange (MLE) reactions to simultaneously introduce polar metal sites and tune pore sizes in the pristine UiO-66 structure. The polar metal sites would serve for

electrostatic interactions while the tuned pore sizes would allow van der Waals interactions in the modified framework of the UiO-66 adsorbent (Hu et al., 2015). All these properties may be very helpful for the adsorptive removal of bulky sulfur contaminants present in JP-8 such as 2,3,7-trimethylbenzothiophene.

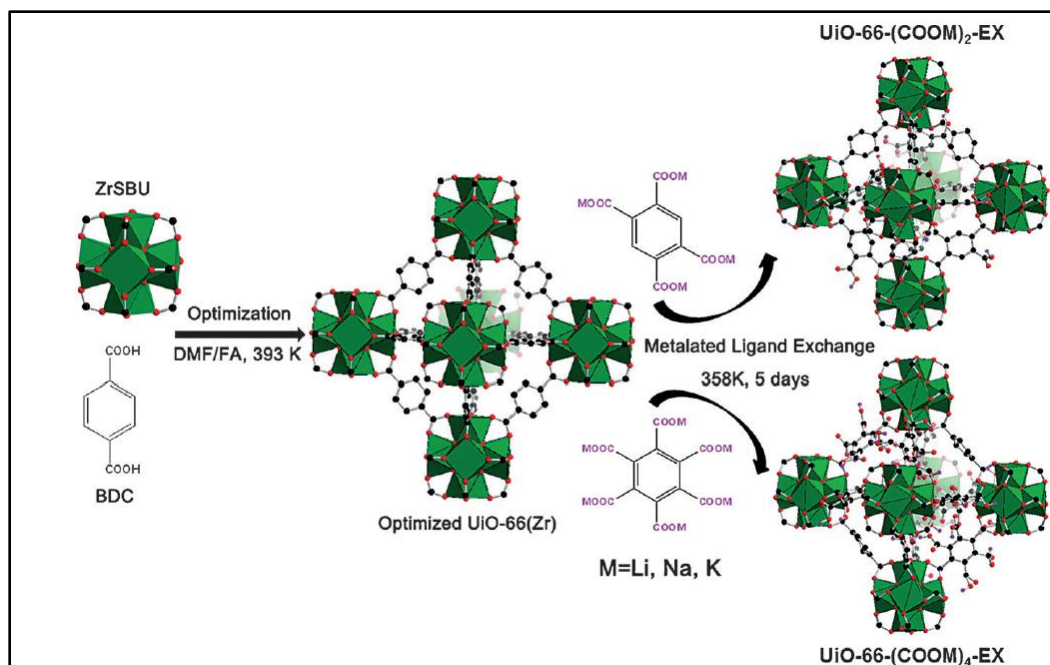


Figure 4.3.3-1. Schematic illustration for the process of optimization and metalated ligand exchange in UiO-66

References

- Amirav, A., & Jing, H. (1995). Pulsed Flame Photometer Detector for Gas Chromatography. *Analytical Chemistry*, 67(18), 3305–3318. <https://doi.org/10.1021/ac00114a030>
- Andrews, A. (2009). Department of Defense Fuel Spending , Supply , Acquisition , and Policy. *CRS Report*.
- Bakshi, K. S., & Henderson, R. F. (1998). Permissible Exposure Levels for Selected Military Fuel Vapors. *Inhalation Toxicology*. <https://doi.org/10.1080/089583798197385>
- Bhandari, V. M., Ko, C. H., Park, J. G., Han, S. S., Cho, S. H., & Kim, J. N. (2006). Desulfurization of diesel using ion-exchanged zeolites. *Chemical Engineering Science*, 61(8), 2599–2608. <https://doi.org/10.1016/j.ces.2005.11.015>
- Chavan, S., Vitillo, J. G., Gianolio, D., Zavorotynska, O., Civalleri, B., Jakobsen, S., ... Bordiga, S. (2012). H₂ storage in isostructural UiO-67 and UiO-66 MOFs. *Physical Chemistry Chemical Physics*, 14(5), 1614–1626. <https://doi.org/10.1039/c1cp23434j>
- Clark, C. A., Heck, K. N., Powell, C. D., & Wong, M. S. (2019). Highly Defective UiO-66 Materials for the Adsorptive Removal of Perfluorooctanesulfonate. *ACS Sustainable Chemistry & Engineering*, 7(7), 6619–6628. <https://doi.org/10.1021/acssuschemeng.8b05572>

- Dias da Silva, P., Samaniego Andrade, S. K., Zygourakis, K., & Wong, M. S. (2019). Adsorptive desulfurization of liquid fuels at elevated temperatures using metal exchanged zeolite Y. *Industrial & Engineering Chemistry Research*, submitted.
- Drake, I. J., Zhang, Y., Briggs, D., Lim, B., Chau, T., & Bell, A. T. (2006). The local environment of Cu⁺ in Cu-Y zeolite and its relationship to the synthesis of dimethyl carbonate. *Journal of Physical Chemistry B*, 110(24), 11654–11664. <https://doi.org/10.1021/jp058245r>
- Fowkes, A. J., Ibberson, R. M., & Rosseinsky, M. J. (2002). Structural characterization of the redox behavior in copper-exchanged sodium zeolite Y by high-resolution powder neutron diffraction. *Chemistry of Materials*, 14(2), 590–602. <https://doi.org/10.1021/cm010504b>
- Furukawa, H., Cordova, K. E., O’Keeffe, M., & Yaghi, O. M. (2013). The chemistry and applications of metal-organic frameworks. *Science*, 341(6149). <https://doi.org/10.1126/science.1230444>
- Gupta, M., Dias da Silva, P., Wellington, S., Wong, M., & Zygourakis, K. (2016). *Patent No. WO2017100617A1*. U.S.A.
- Herna, A. J., & Yang, R. T. (2003). *Desulfurization of Liquid Fuels by Adsorption via π Complexation with Cu(I)-Y and Ag-Y Zeolites*. (I), 123–129. <https://doi.org/10.1021/ie020728j>
- Hernández-Maldonado, A. J., & Yang, R. T. (2004). Desulfurization of Transportation

- Fuels by Adsorption. *Catalysis Reviews*, 46(2), 111–150.
<https://doi.org/10.1081/CR-200032697>
- Hu, Z., Faucher, S., Zhuo, Y., Sun, Y., Wang, S., & Zhao, D. (2015). Combination of Optimization and Metalated-Ligand Exchange: An Effective Approach to Functionalize UiO-66(Zr) MOFs for CO₂ Separation. *Chemistry - A European Journal*, 21(48), 17246–17255. <https://doi.org/10.1002/chem.201503078>
- Kaduk, J.A.; Faber, J. (1995). Crystal structure of zeolite Y as a function of Ion Exchange. *The Rigaku Journal*, 12(2), 14–34.
<https://doi.org/10.5840/ipq2015101249>
- Klein, H., Kirschhock, C., & Fuess, H. (1994). Adsorption and diffusion of aromatic hydrocarbons in zeolite Y by molecular mechanics calculation and X-ray powder diffraction. *Journal of Physical Chemistry®*, 98(47), 12345–12360.
<https://doi.org/10.1021/j100098a033>
- Lee, I. C., & Ubanyionwu, H. C. (2008). Determination of sulfur contaminants in military jet fuels. *Fuel*, 87(3), 312–318.
<https://doi.org/10.1016/j.fuel.2007.05.010>
- Lillerud, K. P., Cavka, J. H., Lamberti, C., Guillou, N., Bordiga, S., Jakobsen, S., & Olsbye, U. (2008). A New Zirconium Inorganic Building Brick Forming Metal Organic Frameworks with Exceptional Stability. *Journal of the American Chemical Society*, 130(42), 13850–13851. <https://doi.org/10.1021/ja8057953>

- Link, D. D., Baltrus, J. P., Rothenberger, K. S., Zandhuis, P., Minus, D. K., & Striebich, R. C. (2003). Class-and structure-specific separation, analysis, and identification techniques for the characterization of the sulfur components of JP-8 aviation fuel. *Energy and Fuels*, *17*(5), 1292–1302. <https://doi.org/10.1021/ef0300747>
- Lobb, J. R. (2017). *Adsorptive Removal of Sulfur-Containing Compounds from Fuels using Metal Loaded Zeolite Y*. Rice University.
- Ma, X., Velu, S., Kim, J. H., & Song, C. (2005). Deep desulfurization of gasoline by selective adsorption over solid adsorbents and impact of analytical methods on ppm-level sulfur quantification for fuel cell applications. *Applied Catalysis B: Environmental*, *56*(1-2 SPEC. ISS.), 137–147. <https://doi.org/10.1016/j.apcatb.2004.08.013>
- O.I. Analytical. (2004). *Model 5380 Pulsed Flame Photometric Detector (PFPD) Operator's Manual*. College Station.
- O.I. Analytical. (2007). *Determination of Total and Speciated Sulfur in Petrochemical Matrices Using a Pulsed Flame Photometric Detector (PFPD)*. *41*(December), 528–534.
- Ragon, F., Horcajada, P., Chevreau, H., Hwang, Y. K., Lee, U. H., Miller, S. R., ... Serre, C. (2014). In situ energy-dispersive x-ray diffraction for the synthesis optimization and scale-up of the porous zirconium terephthalate UiO-66. *Inorganic Chemistry*, *53*(5), 2491–2500. <https://doi.org/10.1021/ic402514n>

- Richter, M., Fait, M. J. G., Eckelt, R., Schneider, M., Radnik, J., Heidemann, D., & Fricke, R. (2007). Gas-phase carbonylation of methanol to dimethyl carbonate on chloride-free Cu-precipitated zeolite Y at normal pressure. *Journal of Catalysis*, 245(1), 11–24. <https://doi.org/10.1016/j.jcat.2006.09.009>
- Shearer, G. C., Chavan, S., Ethiraj, J., Vitillo, J. G., Svelle, S., Olsbye, U., ... Lillerud, K. P. (2014). Tuned to Perfection: Ironing Out the Defects in Metal–Organic Framework UiO-66. *Chemistry of Materials*, 26(14), 4068–4071. <https://doi.org/10.1021/cm501859p>
- Shell Aviation Fuels. (n.d.). *Shell.Com*, 4. Retrieved from <http://www.shell.com/content/dam/shell/static/aviation/downloads/AeroShell-Book/aeroshell-book-2fuels.pdf>
- Toxicologic Assessment of Jet-Propulsion Fuel 8. (2015). In *Toxicologic Assessment of Jet-Propulsion Fuel 8*. <https://doi.org/10.17226/10578>
- Tran, D. T. (2018). Desulfurization of JP-8 jet fuel: challenges and adsorptive materials. *RSC Advances*, 7301–7314. <https://doi.org/10.1039/c7ra12784g>
- Tran, D. T., Palomino, J. M., & Oliver, S. R. J. (2018). Desulfurization of JP-8 jet fuel: Challenges and adsorptive materials. *RSC Advances*, 8(13), 7301–7314. <https://doi.org/10.1039/c7ra12784g>
- Valenzano, L., Civalieri, B., Chavan, S., Bordiga, S., Nilsen, M. H., Jakobsen, S., ... Lamberti, C. (2011). Disclosing the complex structure of UiO-66 metal organic

framework: A synergic combination of experiment and theory. *Chemistry of Materials*, 23(7), 1700–1718. <https://doi.org/10.1021/cm1022882>

Velu, S., Ma, X., & Song, C. (2003). Selective adsorption for removing sulfur from jet fuel over zeolite-based adsorbents. *Industrial and Engineering Chemistry Research*, 42(21), 5293–5304. <https://doi.org/10.1021/ie020995p>

Wang, Yi, Wang, B., Rives, A., & Sun, Y. (2014). Hydrodesulfurization of Transportation Fuels Over Zeolite-Based Supported Catalysts. *Energy and Environment Focus*, 3(1), 45–52. <https://doi.org/10.1166/eef.2014.1088>

Wang, Yuhe, Yang, F. H., Yang, R. T., Con, E., Section, V., Pennsylv, V., & Nickens, A. D. (2006). *Desulfurization of High-Sulfur Jet Fuel by Pi-Complexation with Copper and Palladium Halide Sorbents*. 7649–7655.